Defects in the Self-Assembly of Block Copolymers and Their Relevance for Directed Self-Assembly

Weihua Li[1,2] and Marcus Müller[1]

[1]Institute for Theoretical Physics, Georg-August University, 37077 Göttingen, Germany; email: mmueller@theorie.physik.uni-goettingen.de

[2]Department of Macromolecular Science, State Key Laboratory of Molecular Engineering of Polymers, Fudan University, Shanghai 200433, China

Annu. Rev. Chem. Biomol. Eng. 2015. 6:187–216

First published online as a Review in Advance on April 29, 2015

The *Annual Review of Chemical and Biomolecular Engineering* is online at chembioeng.annualreviews.org

This article's doi: 10.1146/annurev-chembioeng-061114-123209

Keywords

self-assembly, block copolymers, dislocations, disclinations, defect annihilation, chemoepitaxy, graphoepitaxy, minimum free-energy path

Abstract

Block copolymer self-assembly provides a platform for fabricating dense, ordered nanostructures by encoding information in the chemical architecture of multicomponent macromolecules. Depending on the volume fraction of the components and chain topology, these macromolecules form a variety of spatially periodic microphases in thermodynamic equilibrium. The kinetics of self-assembly, however, often results in initial morphologies with defects, and the subsequent ordering is protracted. Different strategies have been devised to direct the self-assembly of copolymer materials by external fields to align and perfect the self-assembled nanostructures. Understanding and controlling the thermodynamics of defects, their response to external fields, and their dynamics is important because applications in microelectronics either require extremely low defect densities or aim at generating specific defects at predetermined locations to fabricate irregular device-oriented structures for integrated circuits. In this review, we discuss defect morphologies of block copolymers in the bulk and thin films, highlighting (*a*) analogies to and differences from defects in other crystalline materials, (*b*) the stability of defects and their dynamics, and (*c*) the influence of external fields.

INTRODUCTION

AB diblock copolymer: a polymer derived from two linear homopolymers (blocks) A and B that are covalently bonded together at their ends

The self-assembly of block copolymers has attracted abiding interest during past decades because it provides a robust and versatile strategy for fabricating dense, ordered structures on the scale of nanometers, which are important for applications ranging from filtration to the manufacturing of microelectronic devices (1–6). The chemical architecture dictates the length scale and symmetry of the nanostructure. Even the deceptively simple AB diblock copolymer, which is composed of two chemically different, linear, flexible chain molecules that are joined at their ends, can form lamellar, hexagonally arranged cylindrical, body-centered-cubic spherical, gyroid, and Fddd phases in the bulk (7, 8) as one varies the volume fraction of the components.

In experiments, however, the single-crystalline periodic microphases typically are not realized, although they represent the minimum of the free energy, i.e., the thermodynamic equilibrium. Instead, a rich variety of defects is observed that results in the formation of polycrystalline morphologies and hence potentially limits the use of block copolymer assembly in applications. Consequently, much effort has been directed toward avoiding the formation of defects and accelerating their annihilation. To devise appropriate strategies, understanding and controlling of the thermodynamics and dynamics of defects are critical.

There are two qualitatively different reasons for the occurrence of defects in block copolymers:

1. In the ultimate vicinity of the order-disorder transition (ODT), the excess free energy, ΔF_{d}, of a defect is comparable to the thermal energy scale $k_{\mathrm{B}}T$, and defects can be conceived as thermal fluctuations around a perfectly ordered state. These equilibrium fluctuations characterize the thermodynamic state and are important to describe the transition from a disordered to an ordered, crystalline state. Most prominently, fluctuations alter the transition in a symmetric, lamella-forming diblock copolymer from second to first order via the Brazovskii mechanism (9), and the ODT in these soft, multicomponent polymer materials shares common features with the crystallization and melting in hard crystals. It is of basic scientific interest to explore the similarities and differences between defects in these soft matter systems and atomic crystals.
2. Outside the vicinity of the ODT, however, the excess free energy of a defect significantly exceeds $k_{\mathrm{B}}T$. In the intermediate segregation regime, $\Delta F_{\mathrm{d}} \gtrsim \mathcal{O}(100k_{\mathrm{B}}T)$ is a typical value for defects in thin films of lamella-forming block copolymers (10). The large excess free energy gives rise to a vanishingly small defect density at thermal equilibrium. Thus, experimentally observed defects cannot be conceived as equilibrium fluctuations around a perfectly ordered state at intermediate or high segregation, but they stem from the kinetics of structure formation.

The large excess free energy results from the fact that, in a dense melt, a collection of many molecules participate in the defect. Their number can be estimated by the dimensionless polymer density, $\sqrt{\overline{\mathcal{N}}} = \frac{\rho_0}{N} R_{\mathrm{e}0}^3$, where ρ_0 denotes the segment number density and N and $R_{\mathrm{e}0}$ are the number of segments per polymer and the end-to-end distance, respectively. The latter quantity also provides an order-of-magnitude estimate for the periodicity of the microphase and the spatial extent of defects. Because the flexible macromolecules adopt random-walk-like conformations, $R_{\mathrm{e}0}^2 \sim N$, the quantity $\overline{\mathcal{N}}$ is proportional to the number of segments. The invariant degree of polymerization typically adopts value of the order $\overline{\mathcal{N}} \sim 10^4$. Therefore, even if the free-energy loss of an individual molecule is only a fraction of the thermal energy scale, the total excess free energy of a defect, ΔF_{d}, will be prohibitive. Because all free energies scale with $k_{\mathrm{B}}T\sqrt{\overline{\mathcal{N}}}$, so does the free-energy barrier, ΔF_{b}, for collective rearrangements that lead to the removal of defects. Thus, in general, defects are long-lived at intermediate and high segregation.

Irrespective of whether defects are equilibrium fluctuations in the ultimate vicinity of the ODT or whether they are metastable states in which the system got trapped in the course of structure formation, their presence limits applications of block copolymer materials. On one hand, the local characteristic dimension or topology of domains at a defect may significantly differ from the perfect structure and thereby affect selective transport through the microphase-separated morphology, which is important for isoporous block copolymer membranes used in filtration applications. On the other hand, defects disrupt the long-range translational and orientational order and are detrimental to the registration of the microphase-separated morphology with boundaries—a property that is critical to applications in microelectronic manufacturing.

The understanding and control of the thermodynamics of defects and the dynamics of defect generation and removal are of fundamental scientific interest and, simultaneously, are important for the development of applications. One strategy to avoid defect formation in the course of self-assembly and to facilitate their removal consists in directing the self-assembly by external fields (4, 11–16). These external fields can be long-range—like electric fields or shear flow—or they can be short range—like chemical guiding patterns on the supporting substrate of a thin film (chemoepitaxy) or geometric substrate features (graphoepitaxy). Long-range fields aim at controlling the overall orientation of the structure on large length scales. Shear (12, 17–26) is frequently used to macroscopically align block copolymer domains in bulk (17) or thin films (4, 16, 27). Angelescu et al. (19) achieved long-range, in-plane order in monolayer-thin films of cylinder-forming copolymers orienting their axis parallel to the shear (19). By a judicious choice of film thickness, bilayer-thick films of sphere-forming copolymers also can be directed to order into a quasi-single-grain structure by shear (20). Alternatively, electric fields have been applied to align block copolymer structure (28–38), exploiting the anisotropy of the free energy of a spatially modulated phase that results from the contrast of dielectric constants between dissimilar blocks (28, 29).

The advantage of shear and electric fields in directing self-assembly is their long-range nature, which affords a manipulation of the structure without explicit guidance on the nanometer length scale. However, it has been difficult to fabricate structures with the excessively low defect densities demanded in many applications of the semiconductor industry. Moreover, these long-range fields control the orientation of the structure but do not break the translation invariance; i.e., they do not necessarily result in registration of the copolymer structure with external boundaries.

Short-range, chemical (chemoepitaxy) (39) or topographical (graphoepitaxy) (40) guiding fields have been employed to direct the structure formation in block copolymers. These two techniques combine the advantages of traditional lithography to fabricate the chemical or topographical guiding pattern with the copolymer's ability to spontaneously form dense, sub-30-nm structures in thin films. Directed self-assembly (DSA)—chemoepitaxy and graphoepitaxy—has become one of the most appealing next-generation lithography techniques, benefiting from reduced feature sizes, integration into the conventional lithographic process flow, low cost, and high throughput. Both strategies have been reviewed recently (4, 11, 13–16).

One of the main tasks of DSA is to fabricate large-scale, defect-free, geometrically simple structures. In principle, this goal can be achieved by destabilizing all possible defects via the presence of the external guiding field and preventing any new defect from forming. Graphoepitaxy directs the ordering by using topographically sculptured substrates, e.g., wide channels (3) or periodically arranged nanoposts (41). The spacing of these topographical substrate features is commensurate with the copolymer periodicity; typically, a small integer multiple not larger than 5 is permissible for defect-free assembly (41). Chemoepitaxy, in turn, directs the self-assembly by chemically patterned substrates that are composed of regions that preferentially interact with

Microphase morphology: spatial arrangement of the different segment species, A and B, on a length scale of 10–100 nanometers, which is set by the size of the polymer molecules

Chemoepitaxy: directed self-assembly by chemically structured substrates, e.g., guiding lines that attract one component of the block copolymer

Graphoepitaxy: directed self-assembly by topographically structured substrates, e.g., grooves

Grain: region with uniform translational and orientational domain order

Directed self-assembly (DSA): self-assembly of materials where the large-scale morphology and orientation are controlled by external forces

one or the other component of the copolymer (39). The periodicity of the guiding pattern may be close to that of the block copolymer. In this case, the advantage of DSA consists of mitigating defects in the chemical guiding pattern and reducing the line-edge roughness by replacing the interfaces of the chemical guiding pattern with internal *AB* interfaces between copolymer domains that are characterized by an interface tension and rigidity. Alternatively, the periodicity of the chemical guiding pattern may be an integer multiple of the copolymer domain spacing. In this case, the copolymer structure multiplies the low spatial frequency of the chemical guiding pattern [density multiplication (42)]. Defect-free assembly is achieved for multiplication factors of approximately 4 in stripe patterns (43, 44) and approximately 3 in hexagonal patterns (45). Guiding patterns with a larger multiple have a lower direction capability and increase the probability of defects.

Another challenging task of DSA consists in manufacturing device-oriented, irregular or aperiodic structures that differ from the bulk phases of block copolymers, e.g., structures that resemble integrated circuits (13, 46–55). Some of these device-oriented structures share many features with prototypical defects. In contrast to the first task, the main objective is to stabilize these useful programmed defects at specified locations.

For both applications of DSA, understanding and controlling defects are critical. To understand the thermodynamics and kinetics of defects in block copolymer materials, it is useful to build on the vast knowledge of defects in atomic crystals and liquid crystalline systems (56, 57) and to draw parallels and highlight differences to these intensively studied materials. The striped morphology in lamellar-forming block copolymers or lying cylinders in a thin film displays smectic order like that in liquid crystals. Likewise, standing cylinders in thin films exhibit hexagonal order that is, for instance, observed in colloid crystals. These similarities not only apply to the spatially modulated phases but also extend to the types of defects, e.g., disclinations, dislocations, and grain boundaries. However, there are also important differences between defects in soft copolymer materials and atomic crystals: (*a*) Whereas the number of atoms or colloids and their size are fixed, the number of domains in a self-assembled copolymer morphology is not constrained by a conservation law. Instead, domains can shrink or expand (58) and be created or destroyed to minimize the excess free energy of a defect in copolymer systems. Even nonbulk morphologies like perforated lamellae may transiently and locally form in the course of defect annihilation (59, 60). (*b*) The internal *AB* interfaces between domains have a spontaneous curvature that can be adjusted by the chain architecture (61, 62). (*c*) In a thin film, there is an interplay between the 2D symmetry of the smectic or hexagonal order and local, 3D structure of intermediates in the course of defect evolution (63). (*d*) The kinetics of defect annihilation is based on the motion of chain molecules in a complex, anisotropic domain structure giving rise to a defect-structure/chain-mobility relationship (60). These additional features of defects in copolymer materials allow them to respond in intriguing ways to geometric confinement and external guiding fields.

In this review, we provide an overview of the structure, thermodynamic stability, and kinetics of defects in the self-assembly of block copolymer materials, highlighting aspects that are relevant to the DSA of copolymer structures in thin films by chemical (chemoepitaxy) or topographical (graphoepitaxy) guiding patterns on the substrates. We focus mainly on basic defect structures that are typical for DSA applications; large composite defects (e.g., fingerprint pattern) are more characteristic of unguided self-assembly on laterally uniform supports. The following section discusses equilibrium properties of defects in stripe and hexagonal patterns as well as grain boundaries and irregular patterns. The section on Dynamics of Defects presents some aspects of the defect motion, defect annihilation, and large-scale grain growth. A brief perspective concludes our review.

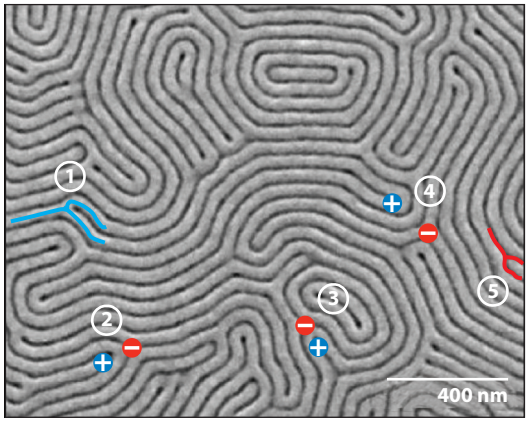

Figure 1

Scanning electron micrograph of the fingerprint morphology formed by solvent annealing of symmetric, lamella-forming PS-b-PMMA thin films. The light and dark domains correspond to polystyrene (PS) and poly(methyl methacrylate) (PMMA) domains, respectively. Five types of defects are indicated: ① PMMA-core dislocation; ② disclination pair: +1/2 PS and −1/2 PMMA; ③ disclination pair: +1/2 PMMA and −1/2 PMMA; ④ disclination pair: +1/2 PMMA and −1/2 PS; and ⑤ PS-core dislocation. The red and blue highlights illustrate the increased connectivity in the PS and PMMA domains, respectively. The scale bar corresponds to 400 nm. Adapted with permission from Reference 69. © 2013 American Chemical Society.

THERMODYNAMIC EQUILIBRIUM PROPERTIES OF DEFECTS

Defects in Stripe Patterns

Stripe patterns are formed either by highly confined, single-layer-thick films of cylinder-forming block copolymers (64–66) or by compositionally symmetric, lamella-forming block copolymers (39, 61, 67–70). In the former systems, the air and the supporting substrate preferentially interact with one of the components, resulting in parallel alignment of the cylindrical minority domains with the substrate. A typical example is a block copolymer comprised of polystyrene (PS) and poly(methyl methacrylate) (PMMA). In the latter systems, the interactions of the block with the supporting substrate and the air must be carefully tuned (71, 72) so that the surface free-energy difference of the two block species is small and standing lamellae perpendicular to the substrate are formed.

Topological defects in these quasi-2D patterns of lines and spaces give rise to splay and bend distortions of the domains similar to what is observed in smectic liquid crystals (56, 57). Most defects are composed of dislocations and disclinations, as illustrated in **Figure 1**, which depicts a typical fingerprint morphology obtained by self-assembly without guiding fields. Often, disclinations appear as pairs with oppositely oriented Burgers vectors (66).

Whereas defect types and geometries in films of lying cylinders and standing lamellae are very similar, the former morphology typically exhibits a faster kinetics of defect annihilation compared with lamellar-forming systems (73). In cylinder-forming systems, a continuous matrix of the majority component gives rise to different diffusion pathways of the polymers from those in lamellar-forming systems (74).

The defect density in experiments depends on the thermodynamic state and annealing conditions (69, 70, 75, 76). The role of increased segregation strength compared to the ODT in the bulk has been studied in cylinder-forming PS-b-poly(2-vinylpyridine) (PS-b-P2VP) copolymers

with molecular weight of 26 kDa within wide channels (75). At a temperature $T = 100°C$, far below the ODT temperature, $T_{ODT} = 212.5 \pm 2.5°C$, in the bulk, excellent orientational order and very low defect density are observed. In this temperature range, defects exclusively consist of dislocations. These isolated point defects are characterized by an excess free energy, ΔF_d. Thus, at any finite temperature, $T > 0$, there exists a finite equilibrium density of dislocations, which is proportional to the Boltzmann factor, $\exp(-\Delta F_d / k_B T)$. The temperature dependence of the defect density yields an estimate of $\Delta F_d \approx 14(1) k_B T$. These dislocations destroy truly long-range positional order of the stripes. For distances greater than $\xi_d \sim \exp(\Delta F_d / 2k_B T)$, a nematic phase is formed instead, which is characterized by quasi-long-range orientational order; i.e., orientational correlations decay like a power law. At higher temperatures, $T > 180°C$, dislocation pairs are created, and their density rapidly increases with T. These topological defects destroy the orientational order, and at $T > 195°C$, only exponentially decaying orientational correlations are observed. Intriguingly, the transition from the nematic to the isotropic, disordered state of the film occurs below the ODT temperature of the bulk.

Qualitatively, these experiments can be nicely described by the theory of melting in a 2D smectic liquid crystal (77), corroborating the universal behavior of defects in block copolymer systems. Quantitatively, the rather large excess free energies, ΔF_d, of defects at intermediate and strong segregation give rise to a large characteristic distance, ξ_d, between defects. Therefore, it is feasible to fabricate smectic order by combing the self-assembly on short distances with chemical or topographical guiding patterns that direct the structure on larger scales than ξ_d.

This insightful study also highlights the critical role of the excess free energy of defects (75). One necessary requirement of DSA is a sufficiently large $\Delta F_d \sim \sqrt{N} k_B T$ so that the defect density in equilibrium is small. This condition is easier to fulfill at large degrees of polymerization. As the critical dimensions of the structures decrease, however, the macromolecules must become shorter. Thus, fewer molecules participate in a defect, thereby decreasing ΔF_d.

Moreover, the excess free energy of dislocations in cylinder-forming systems appears to be smaller than ΔF_d in lamella-forming systems. One of the multiple reasons is that ΔF_d in systems with standing lamellae is proportional to the film thickness. Campbell et al. (70) have observed that defect density in quasi-2D lamellar patterns decreases with the film thickness. Mishra and coworkers (76) have found that the defect density in bilayer patterns of lying cylinders is lower than in monolayer patterns of graphoepitaxially aligned structures thermally annealed at the same temperatures. Additionally, they suggest that the distortion of the unit cell of the cylinders owing to the confinement into thin films shifts the ODT to lower temperatures than the bulk transition temperature (76).

The excess free energy of defects does not depend only on the molecular weight and film thickness. Campbell et al. (61, 69) have systematically investigated the dependence of the PS/PMMA-core ratio in the edge dislocations and disclinations on the compositional asymmetry, f, of the lamella-forming copolymers, revealing that the core type is dictated by the compatibility between the local defect geometry and the interfacial curvature of the corresponding domains. In block copolymers, the internal interfaces between domains are characterized by a spontaneous curvature. If the volume fraction, f, is asymmetric, interfaces prefer to bend toward the minority domain. Because in an edge dislocation the curvature of the end is convex, minority domains preferentially terminate. This effect facilitates the formation of a continuous network of the majority component in a lamellar morphology with defects.

The spontaneous curvature of internal interfaces can be additionally adjusted by chain topology. For example, in compositionally symmetric *ABA* triblock copolymers, which exhibit in many

respects very similar equilibrium properties as symmetric diblock copolymers of half the length (78), experiments observe that domains of the middle *B* block preferentially end (62). Calculations (79, 80) show that the loop-forming middle block, which is anchored with both ends at the *AB* interface, hardly induces a spontaneous curvature, whereas the end block, *A*, bends the internal interface toward the middle domain, *B*, to enlarge the available volume and reduce the stretching of the end blocks. This asymmetry between the middle and end blocks thus gives rise to a spontaneous curvature of the internal interfaces that is in agreement with the experimental findings. Additionally, strategies for tailoring the thermodynamics of defects are discussed in the section on Irregular, Device-Oriented Structures and Defectants.

Ohta-Kawasaki (OK) model: continuum model of microphase separation, where the free energy consists of a local square-gradient functional of the composition and a long-range contribution derived from Leibler's random-phase approximation

Defects in Hexagonal Patterns

Compositionally asymmetric block copolymers form cylindrical or spherical domains in the bulk and have been employed to fabricate 2D hexagonal structures that find applications, for instance, in fabricating quantum dot arrays for lasers (81) or high-density magnetic domains for storage media (82–84). These structures are fabricated by highly confined single-layer-thick films of sphere-forming block copolymers or cylinder-forming block copolymers with balanced surface tensions of both components (58, 85–96).

A hexagonal structure with two dislocation defects is illustrated in **Figure 2**, which was obtained by 2D cell dynamics simulation of a modified Ohta-Kawasaki (OK) model (97). Hexagonal patterns and their defects in block copolymer materials are closely related to 2D triangular solids, e.g., colloidal crystals, which have attracted longstanding scientific interest. Their melting is driven by a thermal generation of dislocation and disclination defects (77, 98–102). Kosterlitz, Thouless, Halperin, Nelson, and Young (99–102) proposed that the melting of a 2D solid occurs in two sequential, continuous transitions—from the solid phase to a hexatic phase and then to a disordered liquid. Two-dimensional triangular solids exhibit only quasi-long-range translational order with an algebraic decay of translational correlations and long-range orientational order because of thermally excited long-wavelength phonons. The transition from this solid to the hexatic phase is driven by the unbinding of dislocation pairs with oppositely oriented Burgers vectors. The hexatic phase is characterized by an exponential decay of translational order but a power-law decay of sixfold orientational order. The melting of this hexatic phase proceeds via the dissociation of disclination pairs [Kosterlitz-Thouless-Halperin-Nelson-Young (KTHNY) theory].

Experiments by Segalman et al. (85–87) have investigated the ordering and melting of a single-layer-thick film of sphere-forming PS-b-P2VP copolymer domains on wide topographical substrate patterns. Most of topological defects are dislocations composed of a pair of a fivefold coordinated site (−60° disclination) and a sevenfold coordinated sphere (+60° disclination) (indicated by the colored lines in **Figure 2*a***). In two dimensions, dislocations spontaneously form and annihilate. An isolated dislocation gives rise to a long-range strain field. Therefore, two dislocations with opposite Burgers vectors form a pair at strong segregation to eliminate the net strain at large distances, reducing the concomitant excess free energy. Upon reducing the segregation strength, dislocation pairs unbind, resulting in a hexatic structure. Even closer to the ODT, dislocations split up into their component disclinations, forming free disclinations. This dissociation of disclination pairs destroys the long-range orientational order in accord with the KTHNY theory for hard, triangular solids (99–102). Best order is obtained by annealing at temperatures close to but below the solid-to-hexatic transition because the ordering kinetics is rapid, yet thermal defect generation is insignificant (86).

Boundaries between grains of different orientations can be described as an array of dislocations. The distance between dislocations increases like the inverse disorientation angle, α, between the

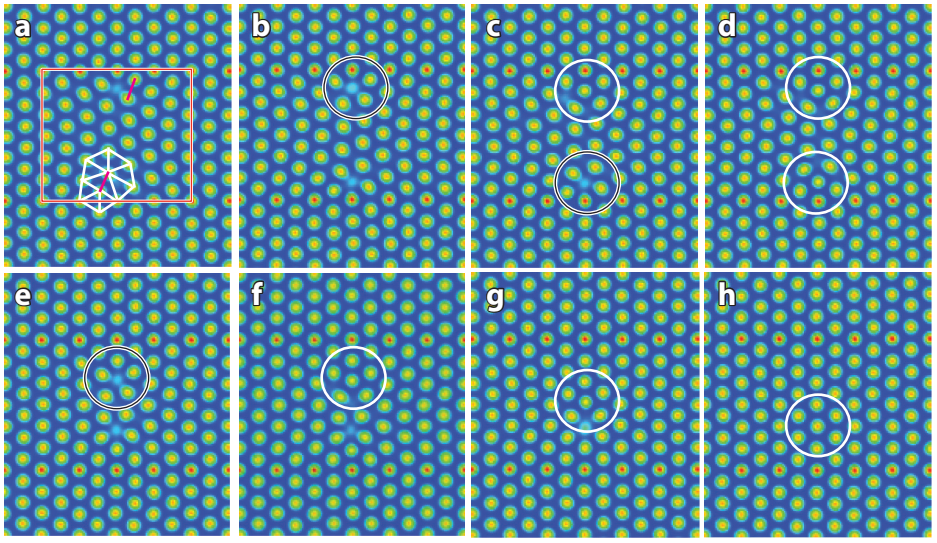

Figure 2

Hexagonal structures and their time evolution predicted by 2D cell dynamics simulation of a modified Ohta-Kawasaki model. Panel *a* indicates two dislocations by short color lines, and the Delaunay triangles around the bottom dislocation identify the fivefold and sevenfold coordinated domains. Subsequent panels correspond to different stages of time evolution, depicting the annihilation of these two dislocations with opposite Burgers vectors guided by a sparse rectangular dot pattern. Black and white circles indicate where a new domain is going to appear or has just come out, respectively. Reprinted with permission from Reference 97. © 2011 AIP Publishing LLC.

grains (89). Vega and coworkers (91) revealed by simulations of the OK free-energy functional the presence of large hexagonal cell superstructures (Moiré patterns) at grain boundaries when the system is in the vicinity of the ODT and the order-order transition to the stripe pattern.

Defects in 3D Bulk Systems

During the self-assembly of block copolymers in the bulk, the long-range order of any ordered phase is unavoidably disrupted by the presence of a variety of grain boundaries that separate ordered domains with different orientations. Defects often accumulate in these grain boundaries, surviving for protracted times and affecting mechanical, transport, and electrical properties.

Grain boundaries in stripe patterns have been studied by experiment (103–109, 110–114) and theory (115–120). The domain structure locally adjusts to minimize the free energy at twist and tilt grain boundaries. At twist grain boundaries, the internal *AB* interfaces form a doubly periodic array of saddle surfaces known as Scherk's first surface (104, 105) or helicoid sections at low twist angle (104, 107). Both are minimal surfaces with zero mean curvature. At tilt boundaries, the domains can be discontinuous (T-junctions) or continuous. The latter ones form chevron shapes at small tilt angles and Ω shapes at larger tilt angles (106, 115, 117). The protrusion at the tip of an Ω grain boundary increases the area of the internal *AB* interface and frustrates the chain packing but reduces the curvature free energy (115).

Whereas grain boundaries are metastable states in bulk systems, they can be stabilized by confinement. Nealey and coworkers (121, 122) have studied the morphology of lamella-forming block copolymers sandwiched between two apposing, stripe-patterned surfaces (chemoepitaxy).

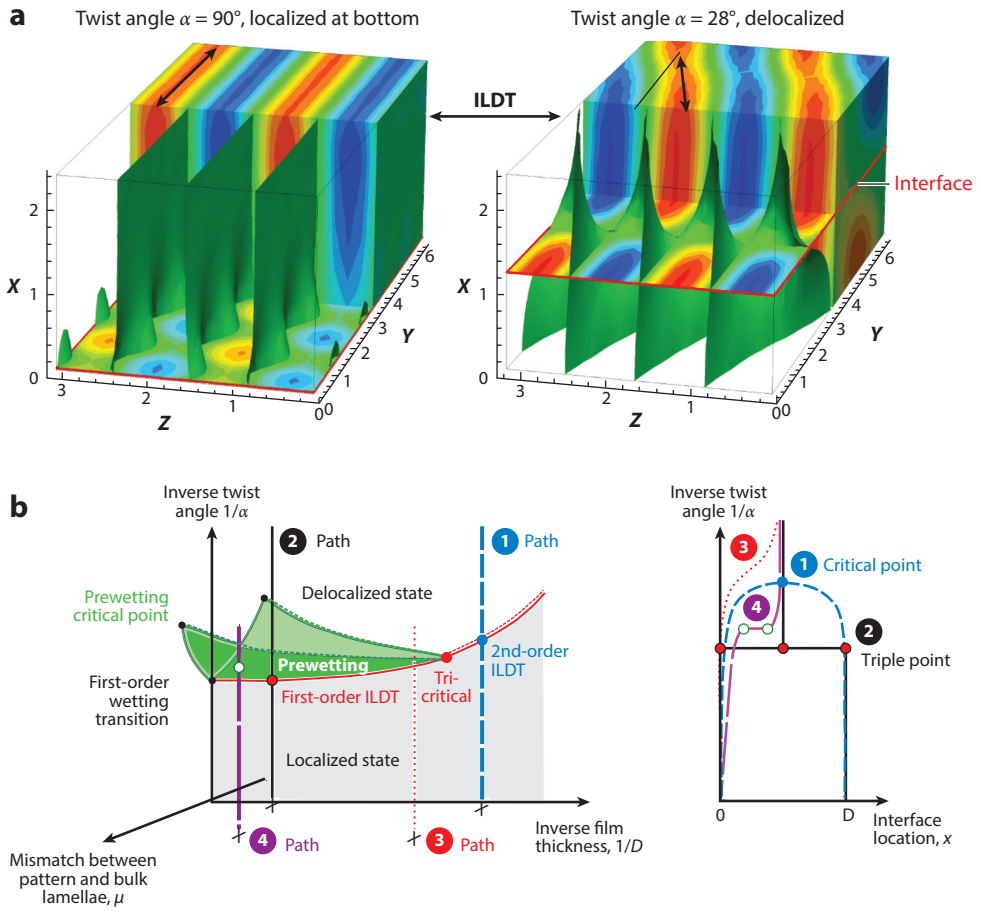

Figure 3

(*top*) Particle simulations of the morphology of a lamella-forming block copolymer between two apposing stripe patterns at distance D apart. Contour plots present the time-averaged composition of the localized and delocalized state for twist angles $\alpha = 90°$ and $\alpha = 28°$, respectively. The position of the twist grain boundary, localized at the bottom substrate, $x \approx 0$, and delocalized in the middle of the film, $x = D/2$ (delocalized), is indicated by a plane. The green surfaces show the internal AB interfaces of the microphase. (*bottom*, *left*) Sketch of the interface localization-delocalization transition (ILDT) as a function of inverse film thickness, $1/D$; inverse twist angle, $1/\alpha$; and period mismatch between the guiding patterns, L_{bottom}, L_{top}, and bulk lamellae, L_0. $\mu \sim [(L_{\text{bottom}} - L_0)^2 - (L_{\text{top}} - L_0)^2]$. Paths ① and ② in the plane $\mu = 0$ correspond to a second- and first-order interface localization-delocalization transition, respectively. $\mu > 0$ for paths ③ and ④. Path ③ does not show any singularity of the interface position, whereas path ④ crosses the surface of prewetting transitions. (*right*) Position x of the interface as a function of $1/\alpha$ for the four paths. Reproduced from Reference 125. © 2012 Am. Phys. Soc.

The chemical stripe patterns on the top and bottom substrate preferentially interact with one component of the copolymer and align and register the lamella morphology at the confining surfaces. The patterns are twisted by an angle α, and a twist grain boundary is formed. **Figure 3** illustrates that this system exhibits an interface localization-delocalization transition (123–125), where the twist grain boundary either is located close to one of the confining surfaces (left, localized state) or fluctuates in the middle of the film (right, delocalized state). The transition between

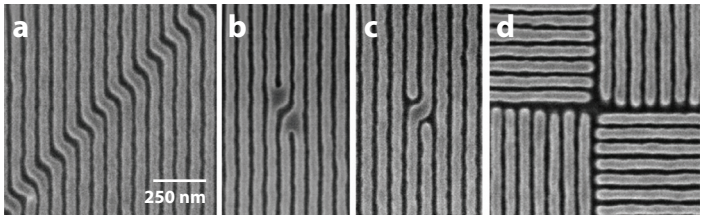

Figure 4

Scanning electron micrography images of a PS/PMMA/PS-b-PMMA ternary blend directed to assemble into (*a*) nested arrays of jogs, (*b*) isolated PMMA jogs, (*c*) isolated PS jogs, and (*d*) arrays of T-junctions. Reprinted with permission from Reference 47. © 2007 Am. Chem. Soc.

those two states can be continuous or abrupt (first-order), and it is closely related to the wetting of the lamellar grain on the chemical guiding pattern. The perpendicular location, x, of the grain boundary can be controlled by the geometrical characteristics of the confinement, which can be directly related to the common thermodynamic parameters of a wetting transition. Temperature corresponds to the twist angle between the apposing surface patterns and the mismatch between the periodicity of the surface pattern, and the bulk morphology of the copolymer material is the analog of the chemical potential. Understanding the interaction of a grain boundary with the confinement and the concomitant wetting phase transitions provides the opportunity to control the 3D structure of the copolymer morphology. Stacking of aligned single-layer templates (126) and functionalized posts in bilayer films (52) has been used to direct the assembly in three dimensions.

Irregular, Device-Oriented Structures and Defectants

The fabrication of basic structural subunits of integrated circuits [including nested arrays of bends and jogs, isolated jogs, and arrays of T-junctions (46)] requires geometric structures that are irregular, isolated, or aperiodic, having no analogs in the bulk-phase diagram of copolymers. **Figure 4** shows that external fields provided by chemoepitaxy have been employed successfully to specify the type and placement of these device-oriented structures in lamellar-forming copolymers (46, 47). Similarly tailored arrays of posts have been employed to direct the assembly of cylinder-forming block copolymers into bends, junctions, and other aperiodic features at specific locations (48, 51). Several theoretical calculations or simulations have been devoted to verifying this method and have aimed to optimize the post array as well as the post shape (48, 49, 53–55). Often the geometry of these device-oriented structures locally resembles defect geometries (e.g., continuous tilt grain boundaries); therefore, it is important to understand how to tailor the excess free energy of defects.

The challenge in fabricating these nonbulk structures involves accommodating spatially varying curvatures and distances between the internal AB interfaces that give rise to packing frustrations (127). For instance, in a nested array of bends (resembling a tilt grain boundary with angle Θ), the distance, $L_C = L_S/\cos(\Theta/2)$, between the internal AB interfaces at the corner of the bend is larger than the distance, L_S, in the lamellar region. The local bend structure can be stabilized by adding A and B homopolymers, which segregate to the corners of the bends and selectively and locally swell the morphology, thereby mitigating the free-energy cost of these irregular structures (46). Alternatively, Kang and coworkers (128) observed an enrichment of nanoparticles at the corners of the bends in copolymer-nanoparticle composites. The localization of nanoparticles at defects has also been observed in self-consistent field theory (SCFT) (129), and Bockstaller and coworkers (114) have experimentally observed the enrichment of filler particles at grain boundaries. This is a universal strategy. Homopolymers and nanoparticles act as defectants (130, 131). In analogy to surfactants that are enriched at a surface, thereby lowering

Self-consistent field theory (SCFT): mean-field approximation of a multicomponent polymer system

the surface tension, defectants segregate to localized nonbulk structures (e.g., the corners of the bends) and lower their excess free energy, thereby reducing the thermodynamic driving force for defect removal and allowing the copolymer material to adopt this irregular structure.

The influence of additives on defect free energies has been investigated by theory (116) and experiment (108). For instance, Burgaz & Gido (108) studied T-junctions in a blend composed of miktoarm star block copolymer, I_2S (I: polyisoprene, S: polystyrene), and PI homopolymer of low molecular weight, observing an increased density of T-junctions compared with continuous tilt grain boundary in pure copolymers. PI domains are always continuous across the grain boundary, whereas the terminating PS lamellae feature enlarged semicylindrical end caps and a concomitant increase of the lamellar spacing at the T-junction (108). This observation can be related to two molecular characteristics: (*a*) The branched architecture of I_2S favors the formation of curved interfaces with the two PI arms being preferentially located on the convex side to reduce crowding. This facilitates the formation of semicylindrical PS end caps. (*b*) The PI homopolymers are preferentially enriched in the high-strain area between the gap of two semicylindrical end caps and the boundary line to mitigate the packing frustration of the PI blocks of I_2S. These examples illustrate how one can encode information about specific nonbulk structures into the molecular architecture of the copolymer material.

Irregular structures can be stabilized by several mechanisms: (*a*) control of the spontaneous curvature of the internal *AB* interfaces by molecular architecture, (*b*) adjustment of the distance between interfaces by local segregation and swelling in multicomponent systems or bridge formation in multiblock copolymers (132), or (*c*) mitigation of packing frustration by polydispersity (133–136). These mechanisms can be inferred from systematically exploring and rationalizing the intriguing multitude of bulk structures that simple two-component *AB* copolymer materials can form when one allows for blending or alternative chain topologies (137, 138). For example, branching in AB_n miktoarm block copolymers can drive the sphere phase to resemble distinct crystal lattices inter alia, the face-centered-cubic phase, the body-centered-cubic phase, the complex σ phase, and the *A*15 phase (132, 139). The impact of the symmetry of the bulk sphere phase on defects in the corresponding monolayer morphology in thin films is an interesting question. When a third component, *C*, is introduced, forming three-component triblock terpolymers, a tetragonal *A*/*C* cylinder phase is stabilized instead of the hexagonal array of cylinders in diblock copolymers (140, 141). The defects in these tetragonal crystals presumably are very different from those in hexagonal lattices. Moreover, SCFT calculations predict a variety of binary cylinder phases when changing the molecular architecture from ABC triblocks to BABCB pentablocks, or ABCB tetrablock copolymers (142), whose defect structures are unexplored.

Thus, there are ample opportunities for exploiting the specific relationship between the molecular characteristics of copolymer materials (e.g., concentration and architecture of defectants) and the structures that they stabilize. The subtle dependence of the bulk structures on the molecular characteristics suggests that the ability of a copolymer material to replicate device-oriented patterns crucially depends on the material properties; i.e., each structure requires a specific fine-tuned mix of defectants. For instance, in the context of chemoepitaxy, a judicious choice of the defectant (homopolymer) concentration is required to fabricate isolated-line structures (47). If one aimed at replicating different, spatially extended patterns on the same wafer (e.g., a mask for electronic circuits), this strategy would rely on the slow, diffusive sorting of defectants, which occurs on a timescale that is significantly longer than the timescale of self-assembly. Thus this strategy of forming programmed defects is limited to high-density structures.

Supramolecular polymer materials that reversibly form and break bonds may help to overcome this difficulty by acting as universal defectants (130, 143). The idea is that the supramolecular material rapidly responds to the DSA guiding pattern and locally and reversibly creates a

defectant mix that allows the copolymer structure to replicate the guiding pattern, eliminating the fine-tuning of the molecular characteristics and the long-range diffusive sorting required for multiple patterns.

Quasi-block copolymers are comprised of *AB* diblock copolymers and supramolecular *B* segments that can reversibly bond to any available *B* terminus on either the copolymers or the *B* oligomers, creating a polydisperse blend of *B* homopolymers and *AB* diblock and *ABA* triblock copolymers (144). A single material is capable of defect-free replication of patterns with perpendicularly crossing, *A*-preferential lines (forming a tic-tac-toe pattern) differing by up to 50% in their length scale (see **Figure 5**). This is a particular challenge because (*a*) the square symmetry has not been observed as a bulk morphology of these quasi-block copolymers; (*b*) the minority component, *A*, forms the continuous matrix phase; (*c*) there is a severe packing frustration where the lines cross; and (*d*) the distance between the internal *AB* interfaces varies across the pattern. The successful DSA is achieved by locally tuning the stoichiometry. For this specific example illustrated in **Figure 5**, the material consists of approximately 90% triblocks, 5% diblocks, and 5% homopolymers, and counterintuitively, the structure with the larger feature size contains shorter *ABA* triblocks than the small-scale structure because the shorter triblocks facilitated the local swelling of the crossing points of lines (130).

DYNAMICS OF DEFECTS

Thermal and Solvent Annealing

In addition to the thermodynamic equilibrium properties, the processing of the block copolymer material or the kinetics of structure formation is important. Typically, thin films are produced by spin coating (145) or solvent casting a polymer-solvent mixture onto a substrate. The solvent evaporates and leaves behind a polymer film with a well-defined film thickness. This process is complex. As the solvent evaporates, the polymer density increases. The concomitant increase in incompatibility, χN, between the components gives rise to microphase separation. The initial condition for this structure formation, however, is ill-defined and presumably depends on material properties and processing conditions. For instance, depending on the polymer-solvent combination and the evaporation rate, the solvent concentration may rapidly decrease at the outer, free surface, resulting in a densification of the polymer at the free surface (skin formation) while leaving the bulk of the film still with high concentrations of solvent (146–148), which results in a spatially inhomogeneous start of the structure formation. Rapid solvent evaporation will additionally give rise to a hydrodynamic flow that may influence structure formation. One might speculate that extremely slow solvent evaporation will result in an initial structure that is characteristic of the thermodynamic state close to ODT, which may feature a smaller periodicity than the equilibrium structure in the absence of solvent. Unfortunately, the kinetics of structure formation in this very initial stage is only incompletely controlled in experiments and only poorly understood by theory. Lacking critical information about the initial condition in experiments, theories and simulations often assume an instantaneous quench from a completely disordered state. In this case, the disordered phase is completely unstable, and structure formation proceeds spontaneously via a spinodal mechanism, which can be tailored, e.g., by confinement effects or external fields. The fastest growing mode of composition fluctuations differs in length scale from the equilibrium domain spacing, resulting in a slight initial strain. This initial stage of structure formation kinetically templates defects, and a better understanding and control of these processes will provide opportunities to optimize DSA by minimizing initial defect densities.

Typically, the initial morphology is riddled with defects, and different annealing strategies—thermal tempering and solvent annealing—have been devised to approach equilibrium, improve

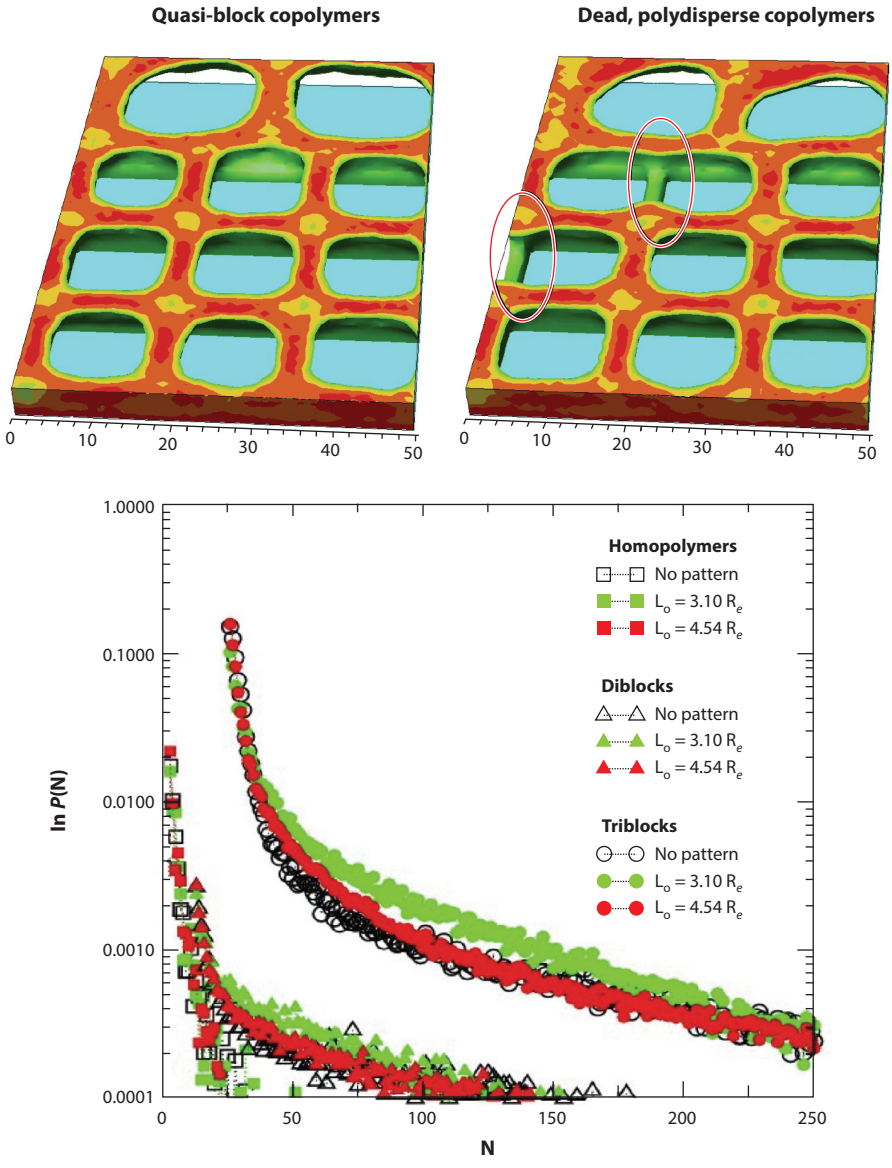

Figure 5

Self-assembly of quasi-block copolymers on a tic-tac-toe pattern with two length scales. The left image depicts the defect-free assembly of quasi-block copolymers, whereas the right image shows the assembled structure with two defects (marked by ellipses) obtained by a polydisperse mixture with the same, but frozen distribution of molecules as the left image. The bottom graph shows the molecular weight distribution of homopolymers, diblocks, and triblocks in the quasi-block copolymer on an unpatterned substrate and two tic-tac-toe patterns with different characteristic lengths, L_0. Reproduced from Reference 130 © 2010 Am. Phys. Soc.

order, and accelerate defect removal. Speeding up the kinetics of structure formation is important for the insertion of DSA of block copolymers into traditional lithographic processes (149).

Flory-Huggins parameter, χ: measure of the incompatibility of monomeric repeat units; the combination χN (N being the number of monomeric repeat units) is an invariant that characterizes the incompatibility of polymers independently from the definition of a monomeric repeat unit

Tempering block copolymer films at elevated temperatures (*a*) increases the chain mobility and (*b*) facilitates the crossing of free-energy barriers in the single-chain and collective dynamics. The former effect benefits from the temperature dependence of the liquid-like molecular packing and the concomitant increase of the chain mobility as temperature is raised above the glass transition temperature. The latter effect gives rise to an Arrhenius behavior of ordering times, $\tau \sim \exp(\Delta F/k_{\mathrm{B}}T)$. The free-energy barrier, ΔF, may stem from the segmental dynamics (e.g., jumps in the torsional potential of consecutive bonds along the molecular backbone), the single-chain kinetics (e.g., diffusion of a block copolymer across lamellar domains), or collective transformations of the domain structure that involve unfavorable intermediates. The latter phenomena are discussed in further detail in the section on Defect Kinetics in Stripe Patterns.

Additionally, a temperature increase may affect the equilibrium thermodynamics of the system by altering the incompatibility, χN, between the blocks or the surface tensions between the blocks and the free surface or the supporting substrate. The latter may result in a different orientation of the microphase, i.e., a switch from a perpendicular to a parallel structure or vice versa.

For PS-b-PMMA block copolymers, the temperature dependence of the Flory-Huggins parameter, χ, and the surface tensions is rather small, whereas for PS-b-P2VP block copolymers, the ODT temperature can be assessed in the temperature interval between the glass transition temperature and the onset of thermal degradation. In this case, a higher annealing temperature corresponds to a smaller incompatibility, χN, and favors a smaller domain spacing, a lower excess free energy of defects, and smaller free-energy barriers of collective transformations of the domain structure.

Solvent annealing alters both the thermodynamics and the dynamics (150). In the simplest case a solvent of low molecular weight swells both domains of the block copolymer material and reduces the incompatibility.[1] This reduces the domain spacing and may result in a tilting of perpendicular domains upon solvent uptake (151). If the solvent exhibits a preference for one of the components, it will alter the volume fractions of the components and may induce a transition to another microphase-separated structure. Solvent concentration may also be enhanced at the substrate and/or the free surface, alter the surface tension, and result in dewetting of a thin supported polymer film (152). The defect structures observed in the course of thermal and solvent annealing are qualitatively similar. For symmetric PS-b-PMMA block copolymers, whose thermodynamics is rather independent of temperature, solvent annealing results in a lower defect density in experiments (69).

Defect Kinetics in Stripe Patterns

Defects are localized deviations from the ideally ordered state that are characterized by an excess free energy, ΔF_{d}. Except for the ultimate vicinity of ODT, however, $\Delta F_{\mathrm{d}} \gg k_{\mathrm{B}}T$, and therefore

[1] By virtue of its large translational entropy, a nonselective, low-molecular-weight solvent rather uniformly distributes in the copolymer film. In this case, the repulsive interactions between the copolymer components are diluted and incompatibility is proportional to the polymer volume fraction, $\chi \sim \phi_{\mathrm{poly}}$. This reduction of incompatibility is enhanced by the tendency of the solvent to enrich at the AB interfaces (175). For larger concentration of solvent, the polymers locally adopt self-avoiding walk statistics, which reduces the unfavorable interactions between distinct blocks even further, $\chi \sim \phi_{\mathrm{poly}}^{1+\frac{1+\nu\omega_{12}}{3\nu-1}}$ where $\nu \approx 0.588$ and $\omega_{12} \approx 0.4$ are the scaling exponent of self-avoiding walks and the correction to scaling exponent that characterizes the contacts of two mutually interdigitating self-avoiding walks, respectively (176–178).

defects are not equilibrium fluctuations but long-lived metastable states into which the kinetics of structure formation has been trapped. Therefore, not only the excess free energy, ΔF_d, but also the mechanisms of defect removal and grain boundary motion and the concomitant free-energy barriers, ΔF_b, of these thermally activated processes are important.

Qualitatively, the initial ordering proceeds via the annihilation of defects and high-energy grain boundaries. This process results in the formation of larger grains with a specific orientation and a low defect density inside the grains. Grain boundaries separate grains with different orientations, and the large-scale coarsening of the grain structure at late stages involves grain-boundary motion. Ryu and coworkers (113) have observed a quasi-stationary grain-coarsening, which is dominated by the annihilation of low-angle continuous tilt grain boundaries, whereas T-junctions and twist grain boundaries are protracted.

Minimum free-energy path (MFEP): path in the free-energy landscape connecting two minima, so that the perpendicular component of the chemical potential vanishes along the path

In the context of DSA, the initial stage of ordering (i.e., grain formation and removal of defects inside a grain) is particularly important because the chemical or topographical guiding patterns dictate the orientation of the structure on large length scales. At intermediate and strong segregations, dislocation dipoles or jogs have a low excess free energy compared with more complex defects; indeed, they are observed during structure formation of lamella-forming block copolymers on chemical stripe patterns (149, 153), in particular when the chemical guiding pattern is slightly narrower than the bulk period (67). Coarse-grained simulations of chemoepitaxy and SCFT calculations of graphoepitaxy (133) show that an incommensurability between the periodicity of the guiding pattern, L_S, or the width of the topographic channel decreases the defect free energy. Dislocations in stripe patterns are also typical defects in thin films of cylinder-forming copolymers that are aligned by topographic patterns (74) or by shear (154).

One computational technique to obtain detailed information about the mechanism of defect removal consists of studying the free-energy landscape, in which the collective ordering kinetics evolves. The minimum free-energy path (MFEP) constructs a sequence of morphologies that connects the defect structure to a perfectly ordered, defect-free structure, such that the free-energy gradient in the direction perpendicular to the path vanishes (155). This method provides a thermodynamic estimate for the most probable path of collective transformations without assuming a reaction coordinate (156, 157). The metastable defect and the perfectly ordered structure are local and global minima of the free-energy profile, respectively, which are separated by one or multiple free-energy barriers, ΔF_b. According to Kramer's transition state theory, the highest barrier, ΔF_b^*, along the defect-removal path dictates the rate of defect removal, $\exp(-\Delta F_b^*/k_B T)$. Because the free-energy landscape of block copolymers is characterized by multiple local minima (158), representing inter alia metastable defects, there may be multiple paths that connect a defect structure to an ordered structure, and the path with the lowest ΔF_b^* will dominate the kinetics.

In the initial stages of ordering, the density of defects is high, giving rise to strong interactions between defects. In this limit, individual defects may not be clearly distinguishable, and the structure changes, implied in their motion and annihilation, may involve complex, spatially extended intermediate structures (59). To quantitatively analyze defect annihilation mechanisms, it is useful to examine the most basic scenarios.

Dislocations with opposite Burgers vectors attract each other via strain-field-mediated interactions. One of multiple important factors setting the timescale of the strain-field-driven defect motion is the self-diffusion coefficient of the polymer because the collective change of structure requires the motion of the constituent polymer molecules. The strain-field-mediated attractions make the two dislocations collide and form a tight disclination dipole, which corresponds to a local minimum of the free energy. The annihilation of this metastable, tight dipole disclination is a thermally activated process that involves breaking and rejoining of domains.

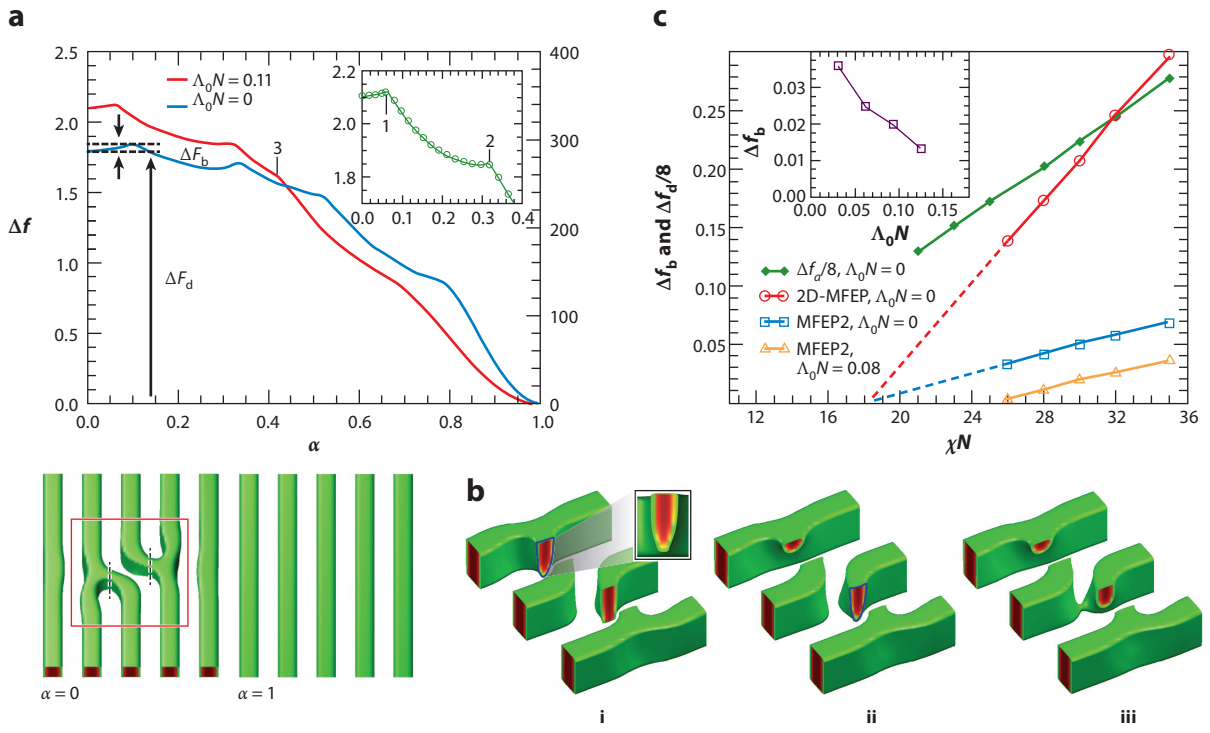

Figure 6

(*a*) Wetting-like defect annihilation mechanism between a tight dislocation pair, $\alpha = 0$, and perfect lamellae, $\alpha = 1$, for $\chi N = 30$ and film thickness D with ($\Lambda_0 N = 0.11$ black line) and without (blue line) guiding pattern. The dimensionless free-energy profile $\Delta f = R_{e0}\Delta F_b / Dk_B T\sqrt{N}$ along the string, α, is shown. The excess free energy, ΔF_d, and the highest energy barrier, ΔF_b^*, are indicated. The inset enlarges the region near the barrier with guiding pattern, $\Lambda_0 N = 0.11$. (b_1), (b_2), and (b_3) Intermediate structures at the barrier, $\alpha \approx 0.059$, and the two shoulders, $\alpha \approx 0.318$ and $\alpha \approx 0.420$, respectively, for the wetting-like mechanism (MFEP2). (*c*) Defect free energy and free-energy barrier for the 2D and wetting-like (MFEP2) mechanism as a function of χN. The inset presents the dependence of Δf_b for the wetting-like mechanism on the strength of the guiding pattern, $\Lambda_0 N$. Reproduced from Reference 63 © 2014 Am. Phys. Soc.

Takahashi et al. constructed the MFEP of removing tight dislocation pairs and disclinations in a graphoepitaxy channel using 2D[2] SCFT (133). Defect removal proceeds by a sequential breaking and rejoining of domains, and the free-energy barrier of the intermediate structures along the path decreases upon lowering the incompatibility, χN. The free-energy barrier, ΔF_b, as a function of the channel width adopts its minimum not when the channel width is commensurate with the bulk lamellar period but when the lamellae are slightly compressed, whereas the defect free energy, ΔF_d, is highest when the lamellae are slightly stretched. Both ΔF_d and ΔF_b increase as the number of lamellae in the channel becomes larger (133).

Li et al. (63) used 3D string calculations to explore defect-removal mechanisms of a dislocation pair on nonpatterned substrates and chemical stripe patterns, as illustrated in **Figure 6**. Along one path, 2D-MFEP, the structures along the MFEP remain uniform perpendicular to the substrate,

[2]The assumption of translational symmetry perpendicular to the substrate, often invoked in self-consistent field calculations and cell dynamics simulations of continuum models (170) for computational reasons, may misrepresent the directing effect of the chemical or topographical guiding pattern.

and, similar to the findings of Takahashi et al. (133), the removal of a *B*-core dislocation dipole proceeds by a lateral motion of the internal *AB* interfaces, sequentially breaking the misaligned *A*-connections and subsequently rejoining the central *A*-domain.

Previous experiments and simulations indicate that in DSA on chemical patterns the order grows from the substrate to the free surface (10, 153). In the 3D string calculations, the sequential breaking of *A*-connections starts at the bottom substrate, forming an aligned defect-free grain at the guiding pattern. This defect-free grain at the substrate is separated by a horizontal grain boundary from the defect structure at the top of the film, qualitatively similar to the grain boundary depicted in **Figure 3**. In this wetting-like mechanism, the thickness of the aligned grain grows, pushing the grain boundary toward the top surface, and the misaligned defect grain at the top becomes thinner (63). Even on a nonpatterned substrate, the free-energy barrier of this wetting-like mechanism is significantly lower than that of the 2D-MFEP (63).

For both mechanisms, 2D-MFEP and wetting-like MFEP, on nonpatterned surfaces, ΔF_{d} and ΔF_{b} decrease approximately linearly with incompatibility in the range $20 \leq \chi N \leq 36$ (63, 133). As the degree of polymerization is decreased (at fixed χ), a significant reduction of the areal defect density has been observed in experiments by Stoykovich and coworkers (70), and this effect has been attributed to a reduced activation free energy for defect annihilation. As expected, the defect free energy ΔF_{d} extrapolates to zero in the vicinity of the ODT, $\chi N_{\mathrm{ODT}} \approx 10.5$. However, the free-energy barrier of defect removal vanishes around $\chi N_* \approx 18$; moreover, this value appears to be independent of the defect removal mechanism, 2D-MFEP or wetting-like MFEP, on nonpatterned substrates. The latter finding suggests that the loss of defect metastability on nonpatterned surfaces is associated with interactions between the distorted, internal *AB* interfaces of the defect. By reducing the segregation, one increases the width of the internal *AB* interfaces. The concomitant range of interactions, which are mediated by the composition profiles across an interface, approaches the domain size hence promoting topological changes of the morphology.

A chemical guiding pattern facilitates the formation of the aligned grain at the substrate and increases the limit, χN_*, of defect metastability, as suggested by the theory of wetting (160). **Figure 6** shows that there exists a range of incompatibilities around χN_* that fulfills two criteria: (*a*) The excess free energy of defects is much larger than the thermal energy scale, $\Delta F_{\mathrm{d}} \gg k_{\mathrm{B}}T$; thus, the probability that a defect spontaneously forms in a defect-free structure is vanishingly small. Note that **Figure 6** indicates that ΔF_{d} can be on the order of $100 k_{\mathrm{B}}T$ at χN_*. (*b*) The free-energy barrier along the path of defect removal vanishes or is comparable to $k_{\mathrm{B}}T$, such that defects are not even metastable. Thus, defects, which have been generated in the course of structure formation, spontaneously annihilate. These thermodynamic conditions are well suited for defect-free DSA (63).

Two dislocations with opposite signs of Burgers vector attract each other owing to long-range strain-field-mediated interactions (161, 162). Thus, these defects will move toward each other and will annihilate according to the above mechanisms upon collision. In smectic liquid crystals and block copolymers, the dislocation motion along the direction of the stripe pattern—climb—is much faster than defect motion across stripes—glide. In the former case, the defect breaks the continuous translational symmetry along the stripes and can move in infinitesimal increments with a vanishingly small free-energy barrier. In the latter case, the dislocation core discontinuously jumps by a (multiple of a) period, requiring a change in the domain connectivity and giving rise to a sizable free-energy barrier (163, 164).

If two dislocations are far apart [precollision regime (165)], the core of the defects is hardly affected by their interaction. The force, F, between dislocations inversely varies with their distance, $F_{\mathrm{dd}} \sim 1/r$, and is proportional to the velocity with which the two dislocations approach each other. Their mutual distance decreases as $r^2(t) = r^2(0) - 8D_{\mathrm{dd}}t$, with time, t (74, 165). The coefficient D_{dd}

is proportional to the mobility of a defect and greatly differs between climb and glide motions. This behavior has been confirmed by experiments (74), and typical coefficients for this driven precollision kinetics are $D_{dd}^{climb} \sim 10^{-12}$ cm^2/s and $D_{dd}^{glide} \sim 10^{-13}$ cm^2/s in thin films of cylinder-forming PS-b-PMMA copolymers of 77 kDa at 240°C.

Swift-Hohenberg model: Landau model of spatially modulated phases characterized by composition fluctuations with wavevectors of a given magnitude

Whereas climb of dislocations does not involve a collective free-energy barrier, it will be protracted if the two dislocations with opposite orientation are strictly apposed along the direction of the stripe pattern. In this special case, an additional domain of length L is formed. The MFEP predicts that the two dislocations approach each other decreasing the free energy linearly with shrinking L. When they collide, they do not even form a metastable state; i.e., there is no collective free-energy barrier in this defect annihilation mechanism (63). Nevertheless, the process is intrinsically slow because the blocks in the extra domain must tunnel through the enclosing opposite domains to remove material from the extra domain, shrinking its length, L. This diffusion process perpendicular to the lamellae exposes the blocks to unfavorable interactions, and the concomitant barrier in the single-chain motion is of the order $f\chi N k_B T$, where f is the volume fraction of the block that forms the extra domain. The equivalent conclusion can be obtained using the local densities of the blocks, ϕ_A and ϕ_B, as collective variables, which is routinely done in time-dependent Ginzburg-Landau (TDGL) calculations. As is found using collective variables, this intrinsic slowness stems not from a collective free-energy barrier but from a small Onsager coefficient, Λ, that relates the thermodynamic driving force—the strain-field-mediated interactions—to a composition current and, via the continuity equation, to a change of local composition. In an incompressible system, $\Lambda \sim \phi_A\phi_B$. Inside the surrounding domain, which the blocks of the extra domain must pass, the product of densities is approximately $\exp(-f\chi N)$; i.e., the thermodynamic driving force does not efficiently translate into a composition change. Note that this special case is analogous to the slowness of climb motion in atomic crystals, where it also involves mass transport.

The motion of disclinations is more complex. It involves the breaking and rejoining of domains and the formation of dislocations (64, 66). Pairs of disclinations with opposite Burgers vectors (see **Figure 7**) exert an attractive force onto each other, but they cannot simply move in response to the force because of the topological constraint imposed by the stripe pattern. The annihilation of a disclination pair produces disclinations to conserve the Burgers vector. Thus, pairwise annihilation of disclinations is suppressed by the topological constraints; instead, the annihilation of disclination quadrupoles, in which the two disclination pairs have opposite Burgers vectors, is frequently observed in experiments and gives rise to a time dependence of the average separation $r^4(t) - r^4(0) \sim t$ (166). **Figure 7** shows that the two complementary quantities—the orientational correlation length, ξ_2, and the interdefect spacing, $\rho_d^{-1/2}$, with ρ_d being the 2D number density of defects—grow like $t^{1/4}$ in a thin film of cylinder-forming PS-b-PI diblock copolymers (166). The experiments are in agreement with simulations of the diblock copolymer lamellar phases described by the Swift-Hohenberg model (167) or by the OK model (168) and 2D smectic-A liquid crystals described by the Landau–de Gennes free-energy functional (169). These experiments have also been corroborated by cylinder-forming PS-b-PMMA thin films, but significantly smaller growth exponents of the characteristic length have been observed in standing lamellae, potentially owing to differences in the geometry (*a*) of transition intermediates involved in breaking and rejoining of domains in the course of defect motion (73) and (*b*) of the pinning of the internal *AB* interfaces at the supporting substrate (68).

The ordering kinetics guided by a sparse stripe pattern has been investigated by using 2D cell dynamic simulations (170). In agreement with experiments (149, 153), the simulations show that the time to achieve defect-free ordering will increase if the incommensurability between stripe pattern and bulk copolymer structure increases. In case of density multiplication by a factor n,

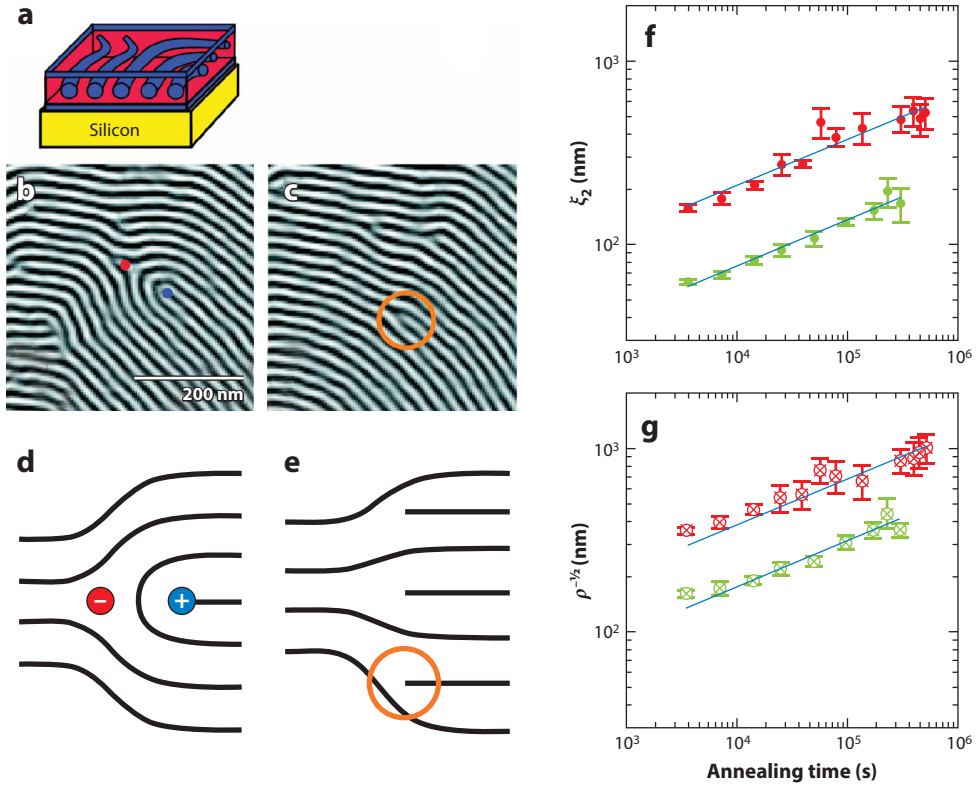

Figure 7

Defects in cylinder-forming PI-b-PS thin films. (*a*) Schematic of the one-layer morphology where the matrix component polystyrene (PS) (*red*) wets both the air and the silicon substrate. (*b*) AFM image of a disclination dipole (+1/2 disclination indicated by the blue circle, −1/2 disclination by the red circle) and additional dislocations. (*c*) The annihilation of a disclination dipole results in multiple disclinations (one of which is indicated by the orange circle). (*d*,*e*) Schematic illustration of the annihilation of a disclination dipole into three dislocations. (*f*) Orientational correlation length, ζ_2, as a function of time for two temperatures, $T =$ 443 K (*red circles*) and 413 K (*green data*), respectively. The solid blue lines are power-law fits to the data, yielding kinetic exponents of 0.25 ± 0.02 at both temperatures. (*g*) The average spacing between disclinations with positive (*circles*) and negative (*crosses*) sign as a function of annealing time for the same system. Power-law fits indicate a kinetic exponent of 1/4. From Reference 166. Reprinted with permission from AAAS.

the simulations indicate an increase of the ordering timescale like n^4, which is consistent with the power law evolution of the correlation length $\xi \sim t^{1/4}$ in the absence of a guiding pattern.

Defect Kinetics in Hexagonal Patterns

The ordering kinetics in hexagonal patterns has been studied by experiment (88) and theory (89, 91, 95, 171–173). Dislocations with opposite Burgers vectors attract each other, causing them to collide and annihilate. Their motion involves the creation and destruction of spherical domains, as illustrated in **Figure 2** (97). In contrast to smectic patterns, however, it is experimentally difficult to follow the motion of individual defects (89). Thus, most studies have focused on the late stages of grain growth. Using 2D simulations of the OK free-energy functional, Yokojima & Shiwa (171)

observed that the characteristic length, ξ_6, of orientational order approximately followed a power-law growth in time with an exponent 1/5 (with or without hydrodynamics). Harrison et al. (88) have carefully investigated the ordering dynamics in a single-layer-thick film of sphere-forming block copolymers in the hexatic regime. Dislocations condense into grain boundaries, and the subsequent coarsening is dictated by the annihilation of small grains. Different measures of the length scale of order have been studied: (*a*) the correlation lengths, ξ_6, of sixfold orientational order; (*b*) the mean distance between disclinations, $\rho_{dc}^{-1/2}$, where ρ_{dc} denotes the number density of free disclinations (i.e., not bound into a dislocation); and (*c*) the mean length of grain boundaries, which is proportional to $1/(p\rho_{dl})$. ρ_{dl} is the number density of dislocations that are almost exclusively located at grain boundaries, and p is the mean distance of dislocations along a grain boundary that remains roughly constant in the absence of grain rotation. Whereas the former correlation length scales like $\xi_6 \sim t^{1/4}$, the latter two quantities exhibit a power law with a smaller exponent of 1/5 (88).

Vega et al. systematically studied the ordering and grain growth in 2D hexagonal systems by TDGL simulations of the OK free-energy functional (89) and compared the results with experiments (88). Free dislocations are typically induced by fluctuations of the orientational order field. The strain fields of isolated dislocations and dislocations bound to small-angle grain boundaries are poorly screened, causing pairs with opposite Burgers vectors to collide and annihilate. Vega's simulations indicate that most of the dislocations cluster to form large-angle grain boundaries. The average distance p between dislocations on large-angle grain boundaries is approximately $2.5a$, where a denotes the lattice spacing, corresponding to an average misorientation of approximately 20°; p only evolves very slowly in time. This value of p also relates to the maximal period of sparse periodic, chemical or topographical guiding patterns for defect-free DSA.

The temporal evolution of polycrystalline patterns in the late stage consists of grain growth, chiefly driven by grain boundary motion. In accord with experiments (88), simulations have observed different power laws for the length scales extracted from the dislocation density and the orientational correlation function, $t^{1/5}$ and $t^{1/4}$, respectively (89). Vega et al. (89) analyzed whether the difference in growth exponents stems from a time dependence of the dislocation distance p along a grain boundary, from grain rotation, or from preferential annihilation of small-angle grain boundaries and favored the latter rational.

The grain boundary motion is driven mainly by the forces acting on triple junctions or forks (89). This force will vanish if the three grain boundaries join at angles of 120°. On very large timescales, grain boundaries between pinned triple junctions straighten, and a logarithmic growth is observed (91, 174).

Li et al. (173) studied the time evolution of defect concentration in hexagonal morphologies consisting of order 10^4 domains guided by a sparse hexagonal field of spots, whose periodicity is an integer multiple, n, of the copolymer period by 2D simulations of the OK free-energy functional. This 2D model mimics density multiplication via a periodic array of nanoposts, which has a directing effect throughout the entire film thickness. **Figure 8** shows that the defect concentration exponentially decays in time for $n \leq 4$, whereas it behaves similarly to unguided structure formation for $n = 6$. For $n = 5$, the evolution of defect concentration initially follows a power law similar to the case $n = 6$ but subsequently decays faster. Analyzing the grain coarsening, Li et al. revealed that the directing effect of the guiding pattern results from preventing the formation of large grain boundaries in the initial stage by registered domains with the guiding pattern. One can observe this effect by comparing the grain distributions of the cases $n = 4$ and $n = 6$ in **Figure 8**. In the initial stage, grains in the case $n = 4$ (panel *c*) are smaller than those for $n = 6$ (panel *d*), resulting in fewer grain boundaries for $n = 4$ (panel *e*) than for $n = 6$ (panel *f*) at later times. The critical multiple around $n = 5$ is closely related to the average distance of dislocations,

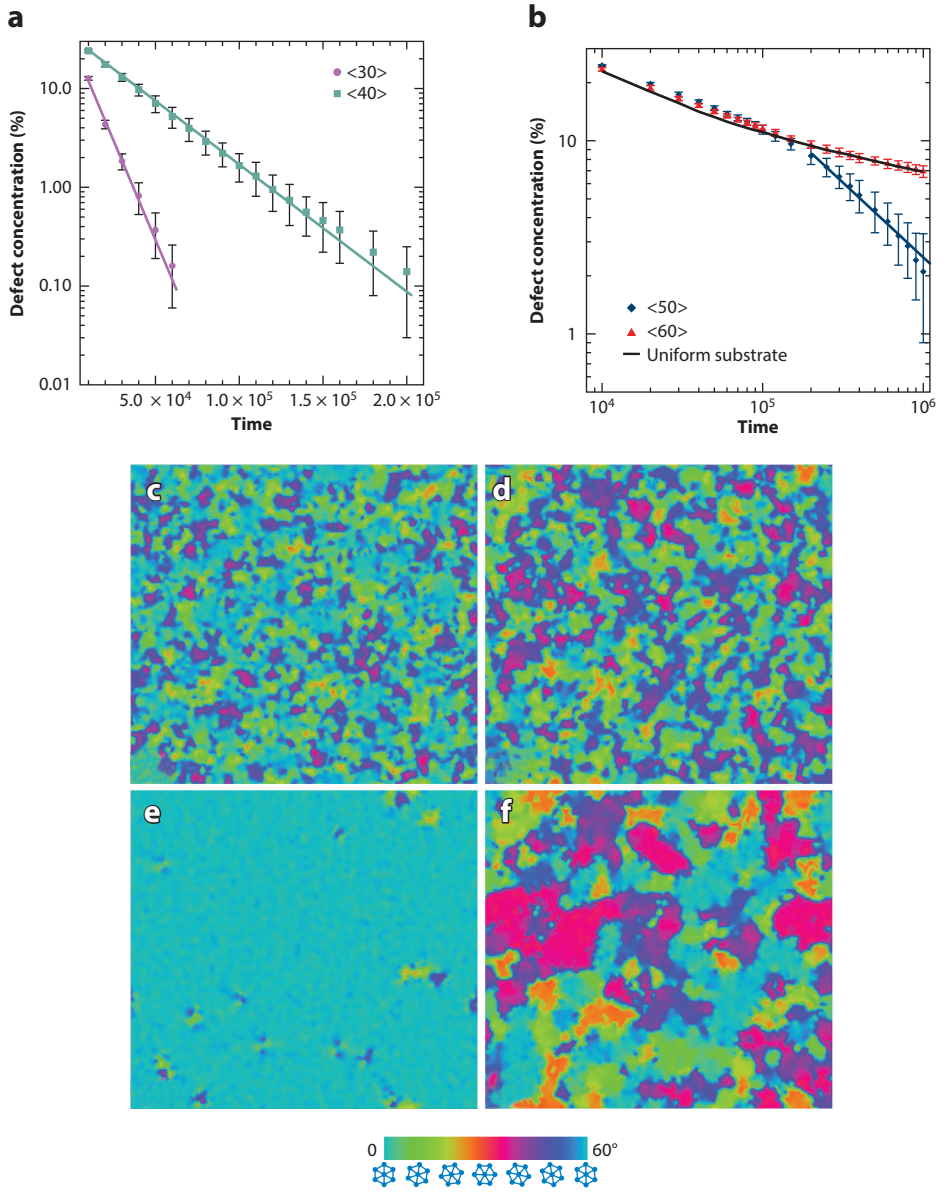

Figure 8

Time evolution of defect concentration of standing cylinders directed by a sparse, hexagonal guiding pattern for various ratios between the cylinder spacing, L_0, in the bulk and the spacing of the guiding pattern, L_S. (*a*) $L_S/L_0 = 3$ and 4, (*b*) $L_S/L_0 = 5$ and 6. Orientational maps of hexagonal domains formed on sparse hexagonal guiding fields with periods of *c* and *e*: $L_S/L_0 = 4$, and *d* and *f*: $L_S/L_0 = 6$. *c* and *d* depict the early stage of coarsening, whereas *e* and *f* correspond to the late stage. The bottom color spectrum indicates the angle range between 0° to 60°. Reprinted with permission from Reference 173 © 2010 Am. Chem. Soc.

approximately 2.5 lattice spacings, without guiding patterns (88, 89). When the spacing between two guiding spots is larger than $n = 5$, the registered domains do not prevent dislocations from clustering into grain boundaries.

PERSPECTIVES

Defects in soft matter, such as copolymer materials or liquid crystals, exhibit a fascinating richness of structures and dynamic properties. At the same time, the understanding and control of these properties are critical for block copolymer lithography, which aims at directing the self-assembly into (*a*) dense, periodic, defect-free structures or (*b*) programmed defects like irregular, device-oriented structures on sub-30-nm scales. In this review, we illustrate the relevance of equilibrium and dynamic properties of defects for DSA of block copolymers.

Whereas the universal aspects of large-scale ordering of 2D stripe and hexagonal structures have attracted abiding theoretical and experimental interest, clarifying the mechanisms of grain growth and grain boundary motion at late stages of ordering and the concomitant power-law growth of the ordering length in time, there remain several open questions that are relevant to DSA:

- The three-dimensionality of the structure, the role of film surfaces, and the interaction with the guiding pattern may allow for additional defect removal mechanisms that differ from the universal, 2D behavior in the absence of guiding patterns. The excess free energy of defects as well as the free-energy barrier of defect removal depend on the film thickness, and the wetting layers of monolayer-thick cylinder or sphere structures influence the collective changes of the domain structure and the diffusion paths of the constituent macromolecules.
- The specific mechanisms by which sparse chemical or topographical guiding patterns align and register the 3D copolymer structure, constrain grain orientation, and interact with defects deserve further investigation. We expect that some of these aspects will depend on the specific types of guiding pattern, chemical or topographical, because they differently influence the 3D copolymer structures.
- Strategies to direct the copolymer structures in three dimensions and to stabilize irregular structure have attracted much less attention than the fabrication of dense, 2D periodic patterns. Additionally, strategies to encode specific defect structures or quadratic or tetragonal structures in the macromolecular architecture must be explored further.
- The role of thermal fluctuations on the stability of defects, their motion, their placement, and their annihilation mechanisms is only incompletely understood. Fluctuation effects will become important for replicating small-scale structures with polymers of lower invariant degrees of polymerization, $\bar{N}$.
- The early stages of structure formation are important for DSA because the guiding pattern directs the spontaneous, spinodal self-assembly. Because these initial structures template defects, controlling these very early stages of self-assembly is critical to minimize the defect density.
- Almost perfect DSA patterns are often characterized by a low density of isolated defects or local defect assemblies. These structures qualitatively differ from the late stages of ordering without guiding fields, which typically consist of large grains separated by grain boundaries, but their ordering mechanisms are less explored.
- The relationship between the kinetics of collective transformations of the domain structure and the underlying motion of the macromolecules is only incompletely understood. Because the diffusion of macromolecules in a spatially modulated structure is much faster parallel than perpendicular to the internal *AB* interfaces, defect annihilation will be significantly

slowed down if it demands perpendicular transport across internal interfaces. Additionally, the role of entanglements and strong dynamic asymmetries between the components of the block copolymer, e.g., owing to different glass transition temperatures, will affect the single-chain dynamics.

DISCLOSURE STATEMENT

The authors are not aware of any affiliations, memberships, funding, or financial holdings that might be perceived as affecting the objectivity of this review.

ACKNOWLEDGMENTS

We have benefited from stimulating collaborations and discussions with K.Ch. Daoulas, J.J. de Pablo, P.F. Nealey, M.P. Stoykovich, R. Shenhar, A.-C. Shi, Y. Tsori, and U. Welling. We thank M.P. Stoykovich and D.A. Vega for thoughtful comments on the manuscript. This work was supported by the European Union FP7 under grant agreement 619793 CoLiSA.MMP (Computational Lithography for Directed Self-Assembly: Materials, Models, and Processes). W.L. additionally thanks the National Natural Science Foundation of China (NSFC) (grants no. 21322407 and no. 21174031) for financial support.

LITERATURE CITED

1. Bates FS, Fredrickson GH. 1990. Block copolymer thermodynamics—theory and experiment. *Annu. Rev. Phys. Chem.* 41:525–57
2. Park C, Yoon J, Thomas EL. 2003. Enabling nanotechnology with self assembled block copolymer patterns. *Polymer* 44:6725–60
3. Segalman RA. 2005. Patterning with block copolymer thin films. *Mater. Sci. Eng. R* 48:191–226
4. Darling SB. 2007. Directing the self-assembly of block copolymers. *Prog. Polym. Sci.* 32:1152–204
5. Hamley IW. 2009. Ordering in thin films of block copolymers: fundamentals to potential applications. *Prog. Polym. Sci.* 34:1161–210
6. Bates FS, Hillmyer MA, Lodge TP, Bates CM, Delaney KT, Fredrickson GH. 2012. Multiblock polymers: Panacea or Pandora's box? *Science* 336:434–40
7. Matsen MW, Schick M. 1994. Stable and unstable phases of a diblock copolymer melt. *Phys. Rev. Lett.* 72:2660–63
8. Tyler CA, Morse DC. 2005. Orthorhombic *Fddd* network in triblock and diblock copolymer melts. *Phys. Rev. Lett.* 94:208302
9. Fredrickson GH, Helfand E. 1987. Fluctuation effects in the theory of microphase separation in block copolymers. *J. Chem. Phys.* 87:697–705
10. Nagpal U, Müller M, Nealey PF, de Pablo JJ. 2012. Free energy of defects in ordered assemblies of block copolymer domains. *ACS Macro Lett.* 1:418–22
11. Kim HC, Park SM, Hinsberg WD. 2010. Block copolymer based nanostructures: materials, processes, and applications to electronics. *Chem. Rev.* 110:146–77
12. Marencic AP, Adamson DH, Chaikin PM, Register RA. 2010. Shear alignment and realignment of sphere-forming and cylinder-forming block copolymer thin films. *Phys. Rev. E* 81:011503
13. Herr DJC. 2011. Directed block copolymer self-assembly for nanoelectronics fabrication. *J. Mater. Res.* 26:122–39
14. Koo K, Ahn H, Kim SW, Ryu DY, Russell TP. 2013. Directed self-assembly of block copolymers in the extreme: guiding microdomains from the small to the large. *Soft Matter* 9:9059–71
15. Bates CM, Maher MJ, Janes DW, Ellison CJ, Willson CG. 2014. Block copolymer lithography. *Macromolecules* 47:2–12

16. Hu H, Gopinadhan M, Osuji CO. 2014. Directed self-assembly of block copolymers: a tutorial review of strategies for enabling nanotechnology with soft matter. *Soft Matter* 10:3867–89
17. Chen Z-R, Kornfield JA, Smith SD, Grothaus JT, Satkowski MM. 1997. Pathways to macroscale order in nanostructured block copolymers. *Science* 277:1248–53
18. Ren SR, Hamley IW, Teixeira PIC, Olmsted PD. 2001. Cell dynamics simulations of shear-induced alignment and defect annihilation in stripe patterns formed by block copolymers. *Phys. Rev. E* 63:041503
19. Angelescu DE, Waller JH, Adamson DH, Deshpande P, Chou SY, et al. 2004. Macroscopic orientation of block copolymer cylinders in single-layer films by shearing. *Adv. Mater.* 16:1736–40
20. Angelescu DE, Waller JH, Register RA, Chaikin PM. 2005. Shear-induced alignment in thin films of spherical nanodomains. *Adv. Mater.* 17:1878–81
21. Luo KF, Yang YL. 2004. Orientational phase transitions in hexagonal cylinder phase and kinetic pathways of lamellar phase to hexagonal phase transition of asymmetric diblock copolymers under steady shear flow. *Polymer* 19:6745–51
22. Arya G, Rottler J, Panagiotopoulos AZ, Srolovitz DJ, Chaikin PM. 2005. Shear ordering in thin films of spherical block copolymer. *Langmuir* 21:11518–27
23. Wu MW, Register RA, Chaikin PM. 2006. Shear alignment of sphere-morphology block copolymer thin films with viscous fluid flow. *Phys. Rev. E* 74:040801
24. Rottler J, Srolovitz DJ. 2007. Mechanism of shear-induced alignment in bilayer thin films of spherical particles. *Phys. Rev. Lett.* 98:175503
25. Marencic AP, Wu MW, Register RA, Chaikin PM. 2007. Orientational order in sphere-forming block copolymer thin films aligned under shear. *Macromolecules* 40:7299–305
26. Pujari S, Keaton MA, Chaikin PM, Register RA. 2012. Alignment of perpendicular lamellae in block copolymer thin films by shearing. *Soft Matter* 8:5358–63
27. Sakurai S. 2008. Progress in control of microdomain orientation in block copolymers—efficiencies of various external fields. *Polymer* 81:2781–96
28. Amundson K, Helfand E, Quan X, Hudson SD, Smith SD. 1994. Alignment of lamellar block copolymer microstructure in an electric field. 2. Mechanisms of alignment. *Macromolecules* 27:6559–70
29. Morkved TL, Lu M, Urbas AM, Ehrichs EE, Jaeger HM, et al. 1996. Local control of microdomain orientation in diblock copolymer thin films with electric fields. *Science* 273:931–33
30. Thurn-Albrecht T, DeRouchey J, Russell TP, Jaeger HM. 2000. Overcoming interfacial interactions with electric fields. *Macromolecules* 33:3250–53
31. Böker A, Elbs H, Hänsel H, Knoll A, Ludwigs S, et al. 2002. Microscopic mechanisms of electric-field-induced alignment of block copolymer microdomains. *Phys. Rev. Lett.* 89:135502
32. Zvelindovsky AV, Sevink GJA. 2003. Comment on "Microscopic mechanisms of electric-field-induced alignment of block copolymer microdomains." *Phys. Rev. Lett.* 90:049601
33. Olszowka V, Kuntermann V, Böker A. 2008. Control of orientational order in block copolymer thin films by electric fields: a combinatorial approach. *Macromolecules* 41:5515–18
34. Pinna M, Schreier L, Zvelindovsky AV. 2008. Mechanisms of electric-field-induced alignment of block copolymer lamellae. *Soft Matter* 5:970–73
35. Zhang JL, Yu XH, Yang P, Peng J, Luo C, et al. 2010. Microphase separation of block copolymer thin films. *Macromol. Rapid Commun.* 31:591–608
36. Liedel C, Hund M, Olszowka V, Böker A. 2012. On the alignment of a cylindrical block copolymer: a time-resolved and 3-dimensional SFM study. *Soft Matter* 8:995–1002
37. Ruppel M, Pester CW, Langner KM, GJA Sevink, Schoberth HG, et al. 2013. Electric field induced selective disordering in lamellar block copolymers. *ACS Nano* 7:3854–67
38. Welling U, Müller M, Shaley H, Tsori Y. 2014. Block copolymer ordering in cylindrical capacitors. *Macromolecules* 47:1850–64
39. Kim SO, Solak HH, Stoykovich MP, Ferrier NJ, de Pablo JJ, Nealey PF. 2003. Epitaxial self-assembly of block copolymers on lithographically defined nanopatterned substrates. *Nature* 424:411–14
40. Segalman RA, Yokoyama H, Kramer EJ. 2001. Graphoepitaxy of spherical domain block copolymer films. *Adv. Mater.* 13:1152–55
41. Bita I, Yang JKW, Jung YS, Ross CA, Thomas EL, Berggren KK. 2008. Graphoepitaxy of self-assembled block copolymers on two-dimensional periodic patterned templates. *Science* 321:939–43

42. Ruiz R, Kang HM, Detcheverry FA, Dobisz E, Kercher DS, et al. 2008. Density multiplication and improved lithography by directed block copolymer assembly. *Science* 321:936–39
43. Cheng JY, Rettner CT, Sanders DP, Kim HC, Hinsberg WD. 2008. Dense self-assembly on sparse chemical patterns: rectifying and multiplying lithographic patterns using block copolymers. *Adv. Mater.* 20:3155–58
44. Liu CC, Ramírez-Hernández A, Han E, Craig GSW, Tada Y, et al. 2013. Chemical patterns for directed self-assembly of lamellae-forming block copolymers with density multiplication of features. *Macromolecules* 46:1415–24
45. Tada Y, Akasaka S, Takenaka M, Yoshida H, Ruiz R, et al. 2009. Nine-fold density muliplication of hcp lattice pattern by directed self-assembly of block copolymer. *Polymer* 50:4250–56
46. Stoykovich MP, Müller M, Kim SO, Solak HH, Edwards EW, et al. 2005. Directed assembly of block copolymer blends into nonregular device-oriented structures. *Science* 308:1442–46
47. Stoykovich MP, Kang H, Daoulas KCh, Liu G, Liu C-C, et al. 2007. Directed self-assembly of block copolymers for nanolithography: fabrication of isolated features and essential integrated circuit geometries. *ACS Nano* 1:168–75
48. Yang JKW, Jung YS, Chang J-B, Mickiwicz RA, Alexander-Katz A, et al. 2010. Complex self-assembled patterns using sparse commensurate templates with locally varying motifs. *Nat. Nanotechnol.* 5:256–60
49. Mickiewicz RA, Yang JKW, Hannon AF, Jung Y-S, Alexander-Katz A, et al. 2010. Enhancing the potential of block copolymer lithography with polymer self-consistent field theory simulations. *Macromolecules* 43:8290–95
50. Chang J-B, Son JG, Hannon AF, Alexander-Katz A, Ross CA, Berggren KK. 2012. Aligned sub-10-nm block copolymer patterns templated by post arrays. *ACS Nano* 6:2071–77
51. Chang JB, Choi HK, Hannon AF, Alexander-Katz A, Ross CA. 2014. Design rules for self-assembled block copolymer patterns using tiled templates. *Nat. Commun.* 5:3305
52. Tavakkoli KG A, Gotrick KW, Hannon AF, Alexander-Katz A, Ross CA, Berggren KK. 2012. Templating three-dimensional self-assembled structures in bilayer block copolymer films. *Science* 336:1294–98
53. Hannon AF, Gotrik KW, Ross CA, Alexander-Katz A. 2013. Inverse design of topographical templates for directed self-assembly of block copolymers. *ACS Macro Lett.* 2:251–55
54. Qin J, Khaira GS, Su Y, Garner GP, Miskin M, et al. 2013. Evolutionary pattern design for copolymer directed self-assembly. *Soft Matter* 9:11467–72
55. Zhang L, Wang L, Lin J. 2014. Harnessing anisotropic nanoposts to enhance long-range orientation order of directed self-assembly nanostructures via large-cell simulations. *ACS Macro Lett.* 3:712–16
56. Gennes PGD. 1969. *The Physics of Liquid Crystals*. Oxford: Clarendon
57. Chaikin PM, Lubensky TC. 1995. *Principles of Condensed Matter Physics*. Cambridge: Cambridge Univ. Press
58. Hammond MR, Sides SW, Fredrickson GH, Kramer EJ. 2003. Adjustment of block copolymer nanodomain sizes at lattice defect sites. *Macromolecules* 36:8712–16
59. Tsarkova L, Horvat A, Krausch G, Zvelindovsky AV, Sevink GJA, et al. 2006. Defect evolution in block copolymer thin film via temporal phase transitions. *Langmuir* 22:8089–95
60. Horvat A, Sevink GJA, Zvelindovsky AV, Krekhov A, Tsarkova L. 2008. Specific features of defect structure and dynamics in the cylinder phase of block copolymers. *ACS Nano* 2:1143–52
61. Campbell IP, Lau GJ, Feaver JL, Stoykovich MP. 2012. Network connectivity and long-range continuity of lamellar morphologies in block copolymer thin films. *Macromolecules* 45:1587–94
62. Ji S, Nagpal U, Liu G, Delcambre SP, Müller M, et al. 2012. Directed assembly of non-equilibrium ABA triblock copolymer morphologies on nanopatterned substrates. *ACS Nano* 6:5440–48
63. Li WH, Nealey PF, de Pablo JJ, Müller M. 2014. Defect removal in the course of directed self-assembly is facilitated in the vicinity of the order-disorder transition. *Phys. Rev. Lett.* 113:168301
64. Hahm J, Lopes WA, Jaeger HM, Sibener SJ. 1998. Defect evolution in ultrathin films of polystyrene-block-polymethylmethacrylate diblock copolymers observed by atomic force microscropy. *J. Chem. Phys.* 109:10111–14
65. Hahm J, Sibener SJ. 2000. Cylinder alignment in annular structures of microsphere-separated polystyrene-*b*-poly(methylmethacrylate). *Langmuir* 16:4766–69

66. Hahm J, Sibener SJ. 2001. Time-resolved atomic force microscopy imaging studies of asymmetric PS-b-PMMA ultrathin films: dislocation and disclination transformations, defect mobility, and evolution of nanoscale morphology. *J. Chem. Phys.* 114:4730–40
67. Kim SO, Kim BH, Kim K, Koo CM, Stoykovich MP, et al. 2006. Defect structure in thin films of a lamellar block copolymer self-assembled on neutral homogeneous and chemically nanopatterned surfaces. *Macromolecules* 39:5466–70
68. Kim BH, Lee HM, Lee J-H, Son S-W, Jeong S-J, et al. 2009. Spontaneous lamellar alignment in thickness-modulated block copolymer films. *Adv. Funct. Mater.* 19:2584–91
69. Campbell IP, He C, Stoykovich MP. 2013. Topologically distinct lamellar block copolymer morphologies formed by solvent and thermal annealing. *ACS Macro Lett.* 2:918–23
70. Campbell IP, Hirokawa S, Stoykovich MP. 2013. Processing approaches for the defect engineering of lamellar-forming block copolymers in thin films. *Macromolecules* 46:9599–608
71. Mansky P, Russell TP, Hawker CJ, Mays J, Cook DC, Satija SK. 1997. Interfacial segregation in disordered block copolymers: effect of tunable surface potentials. *Phys. Rev. Lett.* 79:237–40
72. Peters RD, Yang XM, Kim TK, Sohn BH, Nealey PF. 2000. Using self-assembled monolayers exposed to X-rays to control the wetting behavior of thin films of diblock copolymers. *Langmuir* 16:4625–31
73. Ruiz R, Sandstrom RL, Black CT. 2007. Induced orientational order in symmetric diblock copolymer thin films. *Adv. Mater.* 19:587–91
74. Tong Q, Sibener SJ. 2013. Visualization of individual defect mobility and annihilation within cylinder-forming diblock copolymer thin films on nanopatterned substrates. *Macromolecules* 46:8538–44
75. Hammond MR, Cochran E, Fredrickson GH, Kramer EJ. 2005. Temperature dependence of order, disorder, and defects in laterally confined diblock copolymer cylinder monolayers. *Macromolecules* 38:6575–85
76. Mishra V, Fredrickson GH, Kramer EJ. 2012. Effect of film thickness and domain spacing on the defect densities in directed self-assembly of cylindrical morphology block copolymers. *ACS Nano* 6:2629–41
77. Toner J, Nelson DR. 1981. Smectic, cholesteric, and Rayleigh-Bénard order in two dimensions. *Phys. Rev. B* 23:316–34
78. Matsen MW. 2000. Equilibrium behavior of asymmetric ABA triblock copolymer melts. *J. Chem. Phys.* 113:5539–44
79. Lipowsky R, Döereiner H-G, Hiergeist C, Indrani V. 1995. Membrane curvature induced by polymers and colloids. *Physica A* 249:536–43
80. Müller M, Gompper G. 2002. Elastic properties of polymer interfaces: aggregation of pure diblock, mixed diblock, and triblock copolymers. *Phys. Rev. E* 66:041805
81. Li RR, Dapkus PD, Thompson ME, Jeong WG, Harrison C, et al. 2000. Dense arrays of ordered GaAs nanostructures by selective area growth on substrates patterned by block copolymer lithography. *Appl. Phys. Lett.* 76:1689–91
82. Park M, Chaikin PM, Register RA, Adamson DH. 2001. Large area dense nanoscale patterning of arbitrary surfaces. *Appl. Phys. Lett.* 79:257–59
83. Asakawa K, Hiraoka T, Hieda H, Sakurai M, Kamata Y, Naito K. 2002. Nano-patterning for patterned media using block copolymer. *J. Photopolym. Sci. Technol.* 15:465–70
84. Cheng JY, Ross CA, Thomas EL, Smith HI, Vansco GJ. 2002. Fabrication of nanostructures with long-range order using block copolymer lithography. *Appl. Phys. Lett.* 81:3657–59
85. Segalman RA, Hexemer A, Kramer EJ. 2003. Edge effects on the order and freezing of a 2D array of block copolymer spheres. *Phys. Rev. Lett.* 91:3272–88
86. Segalman RA, Hexemer A, Hayward RC, Kramer EJ. 2003. Ordering and melting of block copolymer spherical domains in 2 and 3 dimensions. *Macromolecules* 36:3272–88
87. Segalman RA, Hexemer A, Kramer EJ. 2003. Effects of lateral confinement on order in spherical domain block copolymer thin films. *Macromolecules* 36:6831–39
88. Harrison C, Angelescu DE, Trawick M, Cheng Z, Huse DA, et al. 2004. Pattern coarsening in a 2D hexagonal system. *Europhys. Lett.* 67:800–6
89. Vega DA, Harrison CK, Angelescu DE, Trawick ML, Huse DA, et al. 2005. Ordering mechanisms in two-dimensional sphere-forming block copolymers. *Phys. Rev. E* 71:061803

90. Kramer EJ. 2005. Melted by mistakes. *Nature* 437:824–25
91. Gómez LR, Vallés EM, Vega DA. 2006. Lifshitz-Safran coarsening dynamics in a 2D hexagonal system. *Phys. Rev. Lett.* 97:188302
92. Aissou K, Baron T, Kogelschatz M, Pascale A. 2007. Phase behavior in thin films of cylinder-forming diblock copolymer: deformation and division of heptacoordinated microdomains. *Macromolecules* 40:5054–59
93. Aissou K, Kogelschatz M, Baron T. 2009. Self-assembling study of a cylinder-forming block copolymer via a nucleation-growth mechanism. *Nanotechnology* 20:095602
94. Liu C-C, Craig GSW, Kang H, Ruiz R, Nealey PF, Ferrier NJ. 2010. Practical implementation of order parameter calculation for directed assembly of block copolymer thin films. *J. Polym. Sci. B Polym. Phys.* 48:2589–603
95. Pezzutti AD, Vega DA, Villar MA. 2011. Dynamics of dislocations in a two-dimensional block copolymer system with hexagonal symmetry. *Philos. Trans. R. Soc. A* 369:335–50
96. Komura M, Komiyama H, Nagai K, Iyoda T. 2013. Direct observation of faceted grain growth of hexagonal cylinder domains in a side chain liquid crystalline block copolymer matrix. *Macromolecules* 46:9013–20
97. Li W, Xie N, Qiu F, Yang Y, Shi A-C. 2011. Ordering kinetics of block copolymers directed by periodic two-dimensional rectangular fields. *J. Chem. Phys.* 134:144901
98. Zippelius A, Halperin BI, Nelson DR. 1980. Dynamics of two-dimensional melting. *Phys. Rev. B* 22:2514–41
99. Young AP. 1979. Melting and the vector Coulomb gas in two dimensions. *Phys. Rev. B* 19:1855–66
100. Nelson DR, Halperin BI. 1979. Dislocation-mediated melting in two dimensions. *Phys. Rev. B* 19:2457–84
101. Halperin BI, Nelson DR. 1978. Theory of two-dimensional melting. *Phys. Rev. Lett.* 41:121–24
102. Kosterlitz JM, Thouless DJ. 1973. Ordering, metastability and phase transitions in two-dimensional systems. *J. Phys. C Solid State Phys.* 6:1181
103. Thomas EL, Anderson DM, Henkee CS, Hoffman D. 1988. Periodic area-minimizing surfaces in block copolymers. *Nature* 334:598–601
104. Gido SP, Gunther J, Thomas EL, Hoffman D. 1993. Lamellar diblock copolymer grain-boundary morphology. 1. Twist boundary characterization. *Macromolecules* 26:4506–20
105. Gido SP, Thomas EL. 1994. Lamellar diblock copolymer grain-boundary morphology. 2. Scherk twist boundary energy calculations. *Macromolecules* 27:849–61
106. Gido SP, Thomas EL. 1994. Lamellar diblock copolymer grain-boundary morphology. 4. Tilt boundaries. *Macromolecules* 27:6137–44
107. Gido SP, Thomas EL. 1997. Lamellar diblock copolymer grain boundary morphology. 3. Helicoid section twist boundary energy. *Macromolecules* 30:3739–46
108. Burgaz E, Gido SP. 2000. T-junction grain boundaries in block copolymer-homopolymer blends. *Macromolecules* 33:8739–45
109. Nishikawa Y, Kawada H, Hasegawa H, Hashimoto T. 1993. Grain boundary morphology of lamellar microdomains. *Acta Polym.* 44:192–200
110. Cohen Y, Albalak RJ, Dair BJ, Capel MS, Thomas EL. 2000. Deformation of oriented lamellar block copolymer films. *Macromolecules* 33:6502–16
111. Jinnai H, Sawa K, Nishi T. 2006. Direct observation of twisted grain boundary in a block copolymer lamellar nanostructure. *Macromolecules* 39:5815–19
112. Listak J, Bockstaller MR. 2006. Stabilization of grain boundary morphologies in lamellar block copolymer/nanoparticle blends. *Macromolecules* 39:5820–25
113. Ryu HJ, Fortner DB, Lee S, Ferebee R, De Graef M, et al. 2013. Role of grain boundary defects during grain coarsening of lamellar block copolymers. *Macromolecules* 46:204–15
114. Ryu HJ, Sun J, Avgeropoulos A, Bockstaller MR. 2013. Retardation of grain growth and grain boundary pinning in athermal block copolymer blend systems. *Macromolecules* 46:1419–27
115. Matsen MW. 1997. Kink grain boundaries in a block copolymer lamellar phase. *J. Chem. Phys.* 107:8110–19

116. Duque D, Schick M. 2000. Self-consistent field theory of twist grain boundaries in block copolymers. *J. Chem. Phys.* 113:5525–30
117. Tsori Y, Andelman D, Schick M. 2000. Defects in lamellar diblock copolymers: chevron- and omega-shaped tilt boundaries. *Phys. Rev. E* 61:2848–58
118. Kyrylyuk AV, Fraaije JGEM. 2005. Three-dimensional structure and motion of twist grain boundaries in block copolymer melts. *Macromolecules* 38:8546–53
119. Boyer D, Viñals J. 2001. Grain-boundary motion in layered phases. *Phys. Rev. E* 63:061704
120. Yoo CD, Viñals J. 2012. Anisotropic linear response in block copolymer lamellar phases. *Macromolecules* 45:4848–56
121. Liu G, Ramírez-Hernández A, Yoshida H, Nygård K, Satapathy DK, et al. 2012. Morphology of lamellae-forming block copolymer films between two orthogonal chemically nanopatterned striped surfaces. *Phys. Rev. Lett.* 108:065502
122. Ramírez-Hernández A, Liu G, Nealey PF, de Pablo JJ. 2012. Symmetric diblock copolymers confined by two nanopatterned surfaces. *Macromolecules* 45:2588–96
123. Parry AO, Evans R. 1990. Influence of wetting on phase equilibria: a novel mechanism for critical-point shifts in films. *Phys. Rev. Lett.* 64:439–42
124. Müller M, Albano EV, Binder K. 2000. Symmetric polymer blend confined into a film with antisymmetric surfaces: interplay between wetting behavior and the phase diagram. *Phys. Rev. E* 62:5281–95
125. Müller M. 2012. Geometry-controlled interface localization-delocalization transition in block copolymers. *Phys. Rev. Lett.* 109:087801
126. García NA, Davis RL, Kim SY, Chaikin PM, Register RA, Vega DA. 2014. Mixed-morphology and mixed-orientation block copolymer bilayers. *RSC Adv.* 4:38412–17
127. Li WH, Müller M. 2015. Directed self-assembly of block copolymers: optimizing molecular architecture, thin-film properties, and kinetics. *Prog. Polym. Sci.* In press
128. Kang H, Detcheverry FA, Mangham AN, Stoykovich MP, Daoulas KCh, et al. 2008. Hierarchical assembly of nanoparticle superstructures from block copolymer-nanoparticle composites. *Phys. Rev. Lett.* 100:148303
129. Kim Y, Chen H, Alexander-Katz A. 2014. Free energy landscape and localization of nanoparticles at block copolymer model defects. *Soft Matter* 10:3284–91
130. Daoulas KC, Cavallo A, Shenhar R, Müller M. 2010. Directed assembly of supramolecular copolymers in thin films: thermodynamic and kinetic advantages. *Phys. Rev. Lett.* 105:108301
131. Kirchheim R. 2009. On the solute-defect interaction in the framework of a defactant concept. *Int. J. Mater. Res.* 100:483–87
132. Xie N, Li WH, Qiu F, Shi AC. 2014. σ phase formed in conformationally asymmetric AB-type block copolymers. *ACS Macro Lett.* 3:906–10
133. Takahashi H, Laachi N, Delaney KT, Hur S-M, Weinheimer CJ, et al. 2012. Defectivity in laterally confined lamella-forming diblock copolymers: thermodynamic and kinetic aspects. *Macromolecules* 45:6253–65
134. Cooke DM, Shi AC. 2006. Effects of polydispersity on phase behavior of diblock copolymers. *Macromolecules* 39:6661–71
135. Schröder-Turk GE, Fogden A, Hyde ST. 2007. Local v/a variations as a measure of structural packing frustration in bicontinuous mesophases, and geometric arguments for an alternating Im $\bar{3}$ m (I-WP) phase in block-copolymers with polydispersity. *Eur. Phys. J. B* 59:115–26
136. Meuler AJ, Ellison CJ, Hillmyer MA, Bates FS. 2008. Polydispersity-induced stabilization of the core-shell gyroid. *Macromolecules* 41:6272–75
137. Matsen MW. 2012. Effect of architecture on the phase behavior of AB-type block copolymer melts. *Macromolecules* 45:2161–65
138. Xu YC, Li WH, Qiu F, Lin ZQ. 2014. Self-assembly of 21-arm star-like diblock copolymer in bulk and under cylindrical confinement. *Nanoscale* 6:6844–52
139. Grason GM, DiDonna BA, Kamien RD. 2003. Geometric theory of diblock copolymer phases. *Phys. Rev. Lett.* 91:058304
140. Matsen MW. 1998. Gyroid versus double-diamond in ABC triblock copolymer melts. *J. Chem. Phys.* 108:785–96

141. Qin J, Bates FS, Morse DC. 2010. Phase behavior of nonfrustrated ABC triblock copolymers: weak and intermediate segregation. *Macromolecules* 43:5128–36
142. Xie N, Liu MJ, Deng HL, Li W, Qiu F, Shi A-C. 2014. Macromolecular metallurgy of binary mesocrystals via designed multiblock terpolymers. *J. Am. Chem. Soc.* 136:2974–77
143. Tang C, Hur S-m, Stahl BC, Sivanandan K, Dimitriou M, et al. 2010. Thin film morphology of block copolymer blends with tunable supramolecular interactions for lithographic applications. *Macromolecules* 43:2880–89
144. Daoulas KC, Cavallo A, Shenhar R, Müller M. 2009. Phase behaviour of quasi-block copolymers: a DFT-based Monte-Carlo study. *Soft Matter* 5:4499–509
145. Flack WW, Soong DS, Bell AT, Hess DW. 1984. A mathematical model for spin coating of polymer resists. *J. Appl. Phys.* 56:1199–206
146. Paradiso SP, Delaney KT, García-Cervera CJ, Ceniceros HD, Fredrickson GH. 2014. Block copolymer self assembly during rapid solvent evaporation: insights into cylinder growth and stability. *ACS Macro Lett.* 3:16–20
147. Münch A, Please CP, Wagner B. 2011. Spin coating of an evaporating polymer solution. *Phys. Fluids* 23:102101
148. Müller M, Smith GD. 2005. Phase separation in binary mixtures containing polymers: a quantitative comparison of single-chain-in-mean-field simulations and computer simulations of the corresponding multichain systems. *J. Polym. Sci. B Polym. Phys.* 43:934–58
149. Welander AM, Kang HM, Stuen KO, Solak HH, Müller M, et al. 2008. Rapid directed assembly of block copolymer films at elevated temperatures. *Macromolecules* 41:2759–61
150. Hur S-M, Khaira GS, Ramirez-Hernandez A, Müller M, Nealey PF, de Pablo JJ. 2015. Simulation of defect reduction in block copolymer thin films by solvent annealing. *ACS Macro Lett.* 4:11–15
151. Rudov AA, Patyukova ES, Neratova IV, Khalatur PG, Posselt D, et al. 2013. Structural changes in lamellar diblock copolymer thin films upon swelling in nonselective solvents. *Macromolecules* 46:5786–95
152. Lin YC, Müller M, Binder K. 2004. Stability of thin polymer films: influence of solvents. *J. Chem. Phys.* 121:3816–28
153. Edwards EW, Stoykovich MP, Müller M, Solak HH, de Pablo JJ, Nealey PF. 2005. Mechanism and kinetics of ordering in diblock copolymer thin films on chemically nanopatterned substrates. *J. Polym. Sci. B Polym. Physics* 43:3444–59
154. Marencic AP, Chaikin PM, Register RA. 2012. Orientational order in cylinder-forming block copolymer thin films. *Phys. Rev. E* 86:021507
155. E W, Ren W, Vanden-Eijnden E. 2007. Simplified and improved string method for computing the minimum energy paths in barrier-crossing events. *J. Chem. Phys.* 126:164103
156. E W, Ren W, Vanden-Eijnden E. 2002. String method for the study of rare events. *Phys. Rev. B* 66:6688–93
157. Maragliano L, Fischer A, Vanden-Eijnden E, Ciccotti G. 2006. String method in collective variables: minimum free energy paths and isocommittor surfaces. *J. Chem. Phys.* 125:024106
158. Zhang C-Z, Wang Z-G. 2006. Random isotropic structures and possible glass transitions in diblock copolymer melts. *Phys. Rev. E* 73:031804
159. Müller M, Li WH, Orozco Rey JC, Welling U. 2015. Defect annihilation in chemoepitaxial directed self-assembly: Computer simulation and self-consistent filed theory. *MRS Proc.* 1750:mrsf14-kk03-05
160. Cahn JW. 1977. Critical-point wetting. *J. Chem. Phys.* 66:3667–72
161. Peach M, Koehler JS. 1950. The forces exerted on dislocations and the stress fields produced by them. *Phys. Rev.* 80:436–39
162. LeSar R. 2014. Simulations of dislocation structure and response. *Annu. Rev. Condens. Matter Phys.* 5:375–407
163. Pershan PS. 1974. Dislocation effects in smectic-A liquid crystals. *J. Appl. Phys.* 45:1590–604
164. Kléman M, Williams CE. 1974. Interaction between parallel edge dislocation lines in a smectic a liquid crystal. *J. Phys. Lett.* 35:49–51
165. Ambrožič M, Kralj S, Sluckin TJ, Žumer S, Svenšek D. 2004. Annihilation of edge dislocations in smectic-*a* liquid crystals. *Phys. Rev. E* 70:051704

166. Harrison C, Adamson DH, Cheng Z, Sebastian JM, Sethuraman S, et al. 2000. Mechanisms of ordering in striped patterns. *Science* 290:1558–60
167. Christensen JJ, Bray AJ. 1998. Pattern dynamics of Rayleigh-Bénard convective rolls and weakly segregated diblock copolymers. *Phys. Rev. E* 58:5364–70
168. Shiwa Y, Taneike T, Yokojima Y. 1996. Scaling behavior of block copolymers in spontaneous growth of lamellar domains. *Phys. Rev. Lett.* 77:4378–81
169. Abukhdeir NM, Rey AD. 2008. Defect kinetics and dynamics of pattern coarsening in a two-dimensional smectic-A system. *N. J. Phys.* 10:063025
170. Xie N, Li WH, Zhang HD, Qiu F, Shi AC. 2013. Kinetics of lamellar formation on sparsely stripped patterns. *J. Chem. Phys.* 139:194903
171. Yokojima Y, Shiwa Y. 2002. Hydrodynamic interactions in ordering process of two-dimensional quenched block copolymers. *Phys. Rev. E* 65:056308
172. Bosse AW, Sides SW, Katsov K, García-Cervera CJ, Fredrickson GH. 2006. Defects and their removal in block copolymer thin film simulations. *J. Polym. Sci. B Polym. Phys.* 44:2495–511
173. Li WH, Qiu F, Yang YL, Shi AC. 2010. Ordering dynamics of directed self-assembly of block copolymers in periodic two-dimensional fields. *Macromolecules* 43:1644–50
174. Safran SA. 1981. Domain growth of degenerate phases. *Phys. Rev. Lett.* 46:1581–84
175. Naughton JR, Matsen MW. 2002. Limitations of the dilution approximation for concentrated block copolymer/solvent mixtures. *Macromolecules* 35:5688–96
176. Müller M, Binder K, Schäfer L. 2000. Intra- and interchain correlations in semidilute polymer solutions: Monte Carlo simulations and renormalization group results. *Macromolecules* 33:4568–80
177. Olvera de la Cruz M. 1989. Theory of microphase separation in block copolymer solutions. *J. Chem. Phys.* 90:1995–2002
178. Joanny JF, Leibler L, Ball R. 1984. Is chemical mismatch important in polymer-solutions? *J. Chem. Phys.* 81:4640–56

Annual Review of Chemical and Biomolecular Engineering

Volume 6, 2015

Contents

Indexes

Errata

An online log of corrections to *Annual Review of Chemical and Biomolecular Engineering* articles may be found at http://www.annualreviews.org/errata/chembioeng